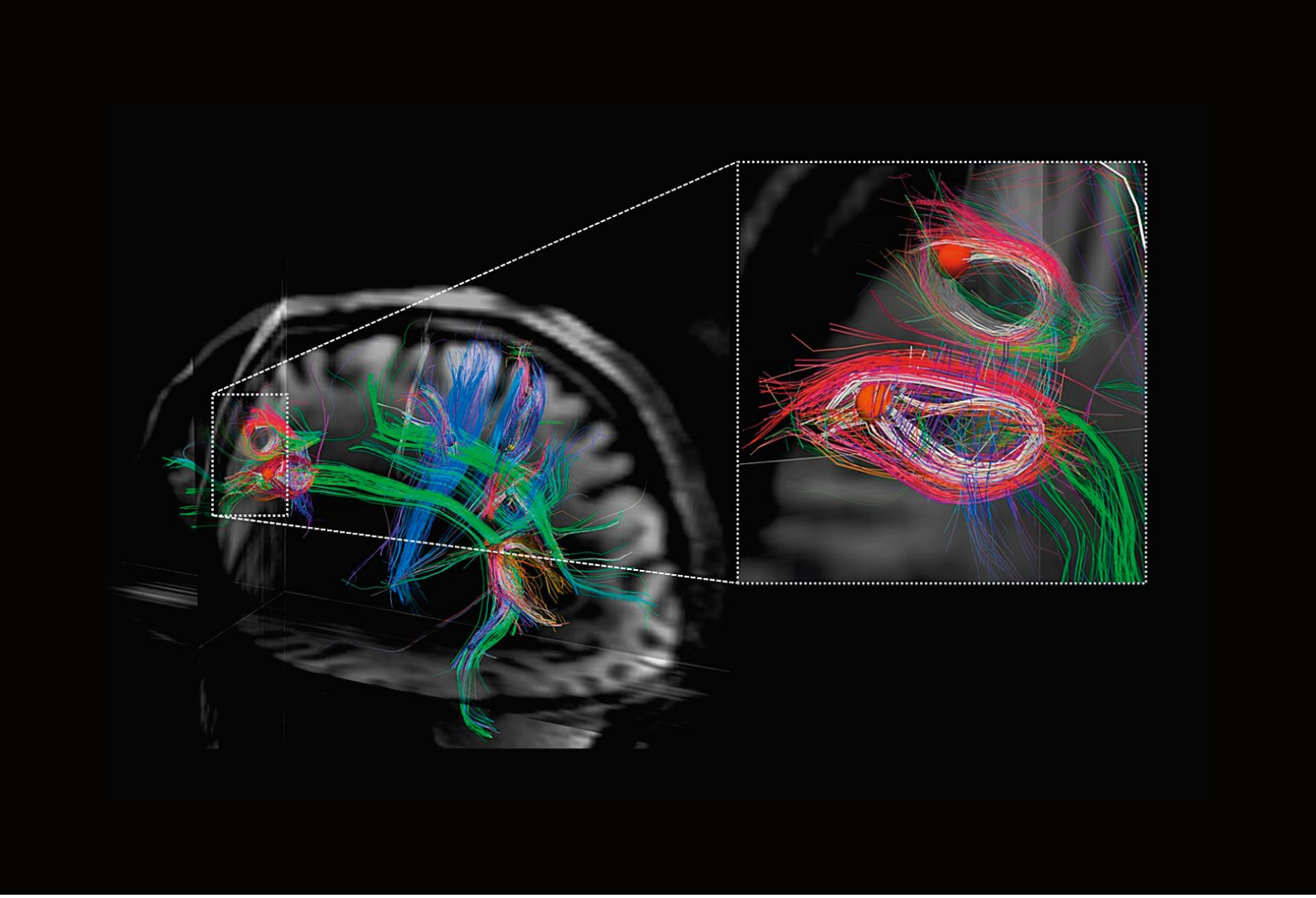

Pioneers of Gradient Systems

An Attempt to Reconstruct the History of Gradient-System Technology at Siemens Healthineers

Franz Schmitt; Stefan Nowak; Eva Eberlein
Siemens Healthineers, Erlangen, Germany

Pioneers of Connectome Gradients

Ralph Kimmlingen
Siemens Healthineers, Erlangen, Germany

siemens-healthineers.com/magnetom-world

SIEMENS Healthineers

An Attempt to Reconstruct the History of Gradient-System Technology at Siemens Healthineers

Franz Schmitt; Stefan Nowak; Eva Eberlein

Siemens Healthineers, Erlangen, Germany

Reprinted from MAGNETOM Flash (77) 2/2020

Introduction

The development of clinical MRI was a journey into engineering terra incognita. Although the basic components were known through building MRI prototypes in the early 1980s [1], driving this technology to perfection demanded innovations aplenty. Entirely new technological paths had to be navigated to perfect magnets, gradients, and RF excitation and reception.

This article explores how Siemens Healthineers learned to make good gradients. It charts the amazing technological advances from 1983, when Siemens Medizintechnik, as it was called then, began to develop their first MRI product, the MAGNETOM; until today, when Siemens Healthineers provide MAGNETOM Prisma, MAGNETOM Terra, and MAGNETOM Connectom[1] to the clinical and research community.

To get the story straight, we have revisited old memos and lab books, and consulted colleagues from the early days of MR at Siemens and also other companies. Technological progress comes through the ingenuity of many people, so we also tell the personal stories that reveal why one and not another path was taken.

[1] *MAGNETOM Connectom is ongoing research. All data shown are acquired using a non-commercial system under institutional review board permission. Siemens Healthcare GmbH does not intend to commercialize the system.*

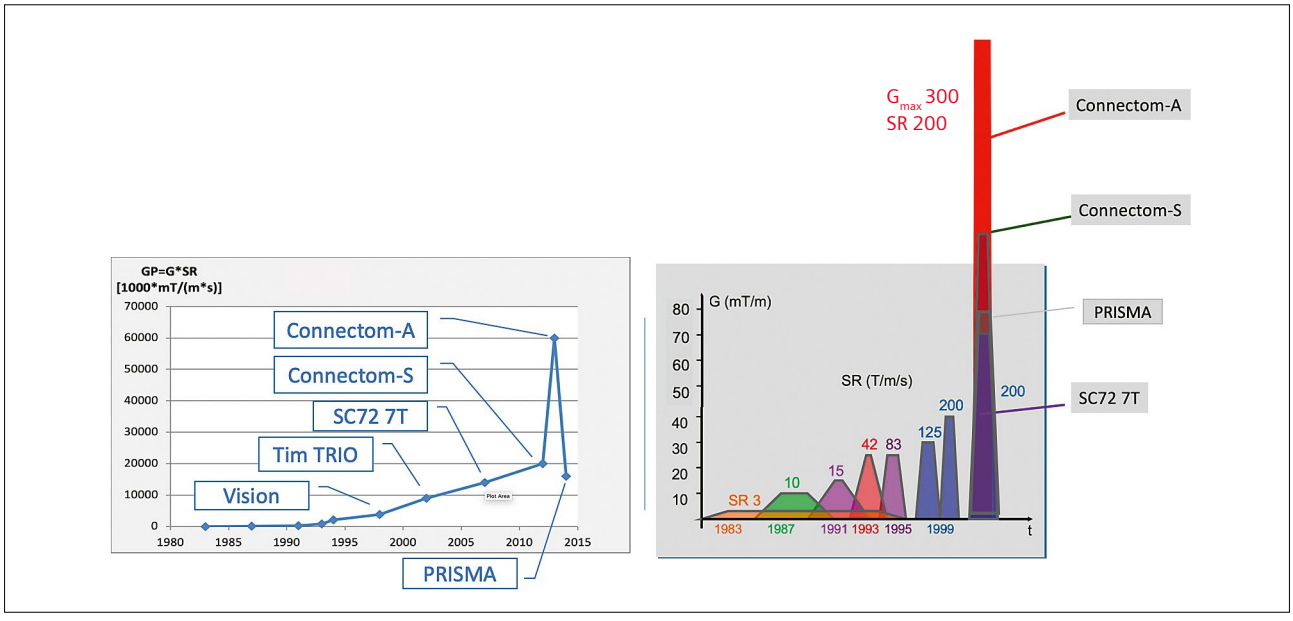

1 Evolution of gradient performance.

Gradient performance over the years

Since the introduction of MRI as a commercially available diagnostic tool in 1983, dramatic improvements have been achieved in all features defining image quality, such as resolution, signal-to-noise ratio (SNR), and speed. Initially, spin echo (SE) images with 128 x 128 pixels per slice were acquired in several minutes. Nowadays, the standard matrix size for musculoskeletal and neuro studies using TSE-based techniques is 512 x 512 with similar imaging times, but covering the entire volume of interest. Echo-planar imaging (EPI) [2] techniques has made it possible to acquire 128 x 128 images in less than 100 ms. Most recently, Simultaneous Multi-Slice (e.g., SMS-EPI for BOLD fMRI) allows the acquisition of an entire volume of 100 slices with resolution of $(1.2\ mm)^3$ at a repetition time (TR) of 1.3 seconds. That is CT-like speed [3, 4]. Here, high-speed gradients and novel RF excitation and reception techniques are combined, allowing resolution and throughput only dreamed of a few years ago.

At the beginning of clinical MRI, maximum achievable gradients G_{max} were typically in the range of 1 to 2 mT/m amplitude, with rise times of 1 to 2 ms. In terms of slew rate (SR), in units of T/m/s, that is on the order of SR 1. Over almost four decades, amplitudes and slew rates have increased by orders of magnitude. Present-day technology provides gradient pulses up to 80 mT/m for whole-body applications, with SR 200 T/m/s. This slew rate is the physiological limit for peripheral nerve stimulation (PNS) in whole-body applications, but not a technical limit. The slew rate is regulated by PNS thresholds [13]: When shortening a pulse sequence, the regulatory limits of PNS need to be observed. Higher SR is possible through higher voltages in principle, although it would present other technical challenges such as high voltage resilience of the entire gradient system. More on this later.

By reducing the linearity volume of a gradient coil, faster switching at higher amplitudes is possible. This has been introduced with the MAGNETOM Sonata [5] and with the SC72 gradient coil (70 mT/m at SR 200 T/m/s) in our 7T whole-body system [6]. This development has been pushed furthest for the Human Connectome project [7–9], with two gradient systems: the Connectom-S, a redesign of the SC72 for the 3T MAGNETOM Skyra magnet performing with 100 mT/m at SR 200 T/m/s; and the Connectom-A, also for the MAGNETOM Skyra magnet, which has a peak performance of 300 mT/m at SR 200 T/m/s [10]. Both systems sacrificed the patient bore, reducing it to 580 mm diameter.

So the performance of gradient systems has improved enormously. The product of maximum gradient strength times the slew rate, $GP = G_{max} * SR$, reflects the gradient performance GP [11]. The entire evolution of gradient performance is demonstrated in Figure 1.

Gradient and its leading role in fast MRI

Before we dive deeper into the technological intricacies of gradient systems, let's have a look what the major drivers of gradient performance were over the years.

First, the attainable spatial resolution in MRI (δx, the pixel size) is inversely proportional to the gradient-time integral

Equation 1

$$\delta x = \frac{2\pi}{\gamma \int G(t)dt}$$

integrated over the readout period T_{RO} (Fig. 2A), with γ representing the gyromagnetic ratio. Please note that integration is over the entire RO gradient pulse including the up and down ramp, and simultaneous acquisition of the MR signal: an extreme case, usually used for EPI, to show the need for higher and faster gradients. To shorten T_{RO} for a particular MR pulse sequence type without sacrificing resolution, the gradient amplitude G_{RO} must increase, and rise time T_{Rise} decrease.

Note the gyromagnetic ratio γ in the denominator of Equation 1. The vast majority of MRI is performed with protons, but with emerging ultra-high fields, such as 7T, other nuclei such as Sodium (^{23}Na) are becoming interesting [12]. As these nuclei have lower gyromagnetic ratio, gradient amplitude must be increased to maintain resolution.

When shortening gradient pulses, the limit to gradient amplitude is not set by technical feasibility, but mainly by the SNR, as extremely high bandwidth while acquiring the MR signal results in poor SNR:

Equation 2

$$SNR \sim \sqrt{\frac{1}{BW}}$$

A fast GRE example is shown in the lowest part of Figure 2B, illustrating the benefits of faster and stronger gradients to achieve shorter echo times (TE).

The development of echo-planar imaging (EPI) required extreme gradient performance (Fig. 2C). While normal SE and GRE imaging techniques could easily live with 10 T/m at SR 50 T/m/s or even below, EPI for neuro applications requires 30 mT/m and SR of 200 T/m/s in order to gather the T2*-weighted MR signal with a decent SNR, and minimize susceptibility artifacts.

Second, gradient power far beyond even EPI requirements became desirable when diffusion-weighted MR Imaging (DWI) was developed. For DWI, usually in combination with an EPI readout, strong and short gradient pulses, as described with the Stejskal-Tanner pulse scheme [14], yield high b-values in the shortest possible time to optimize SNR (Fig. 3). Until 2012,

the MR community used 45 mT/m at SR 200 T/m/s. Then the introduction of the Connectom gradients, which provided up to 300 mT/m at SR 200 T/m/s for experimental purposes, spurred the major vendors to improve their clinical scanners to 80 mT/m peak gradient strength, reflecting the needs of high-resolution MR diffusion imaging techniques such as diffusion spectral imaging (DSI) [15]. SNR in diffusion-weighted imaging can thereby improve considerably (Figure 3 left). The MGH group headed by Lawrence Wald and Van Wedeen showed a 3-fold SNR boost compared with G_{max} = 40 mT/m, which is excellent for an SNR-weak technique such as diffusion-weighted MRI (see Figure 3 right).

Third, moving from unshielded to shielded gradients, the number of wires almost doubles and the inductance slightly increases, resulting in a lower sensitivity (G/I_G) with G the gradient strength reached with a certain current I_G. Thus higher voltage and currents are needed to drive a gradient coil for given G_{max} and SR_{max}. That explains in part the historic performance increase in the first decade of clinical MRI, from 120 V_{peak} / 150 A_{peak} for the MAGNETOM (i.e. the first-generation Siemens MR system) and 250 V / 160 A_{peak} for the MAGNETOM SP (both with unshielded gradient coils) to the MAGNETOM Impact (shielded) which needed 300 V / 250 A_{peak} power supplies.

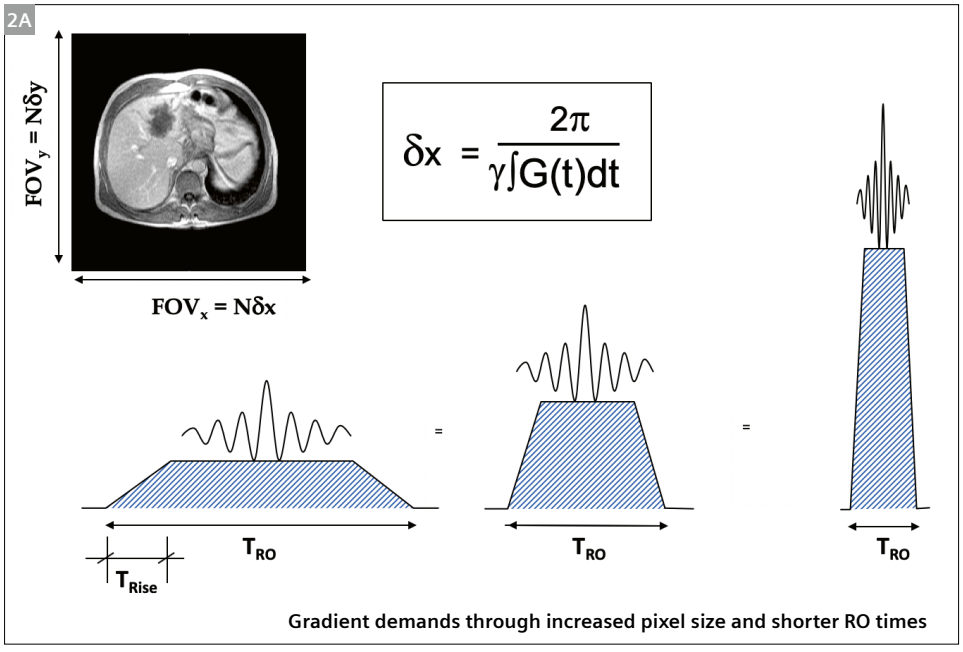

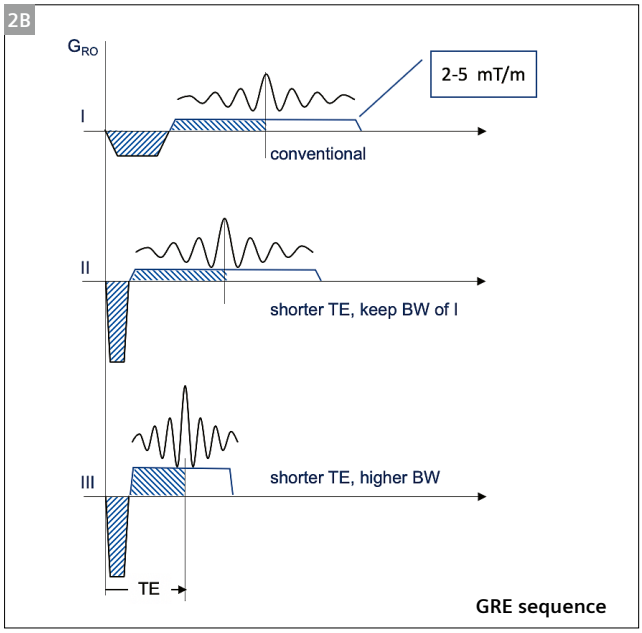

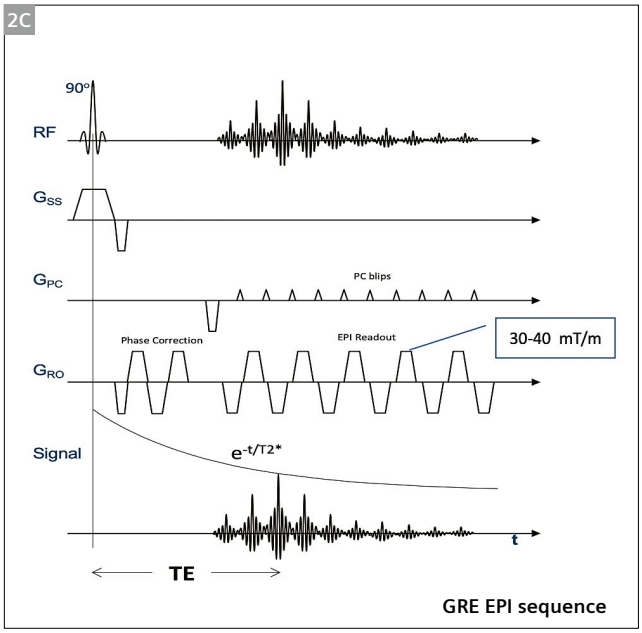

2 **(2A)** Image resolution and its correlation to the gradient-time integral. Gradient amplitude G_{RO} and slew rate must increase to maintain resolution while shortening T_{RO}. Lower row: increasing amplitude and slew rate is the key to shorter TE. **(2B)** Shortening a readout pulse with pre-dephaser to increase speed, with and without changing signal BW. **(2C)** Typical EPI pulse sequence timing.

Forth, the trend to shorter and wider MR systems also has to be noted here. The power required for a given gradient performance is approximately proportional to r^5 [16] where r represents the radius of the gradient coil. This is reflected in the higher currents provided by gradient power amplifiers in the last 15 years, since the MAGNETOM Espree (70 cm bore diameter with a length of 1.2 m) was introduced. The first Siemens 70 cm wide-bore 3T system, the MAGNETOM Verio, provided 2250 V / 900 A_{peak}, while the very successful MAGNETOM Trio with its 60 cm bore needed only 2000 V / 650 A_{peak}. Now, with the XT gradients of the MAGNETOM Vida (70 cm bore size), 2250 V / 1200 A are available to match modern MR imaging requirements. One thing is for sure: the electricity bill is increasing.

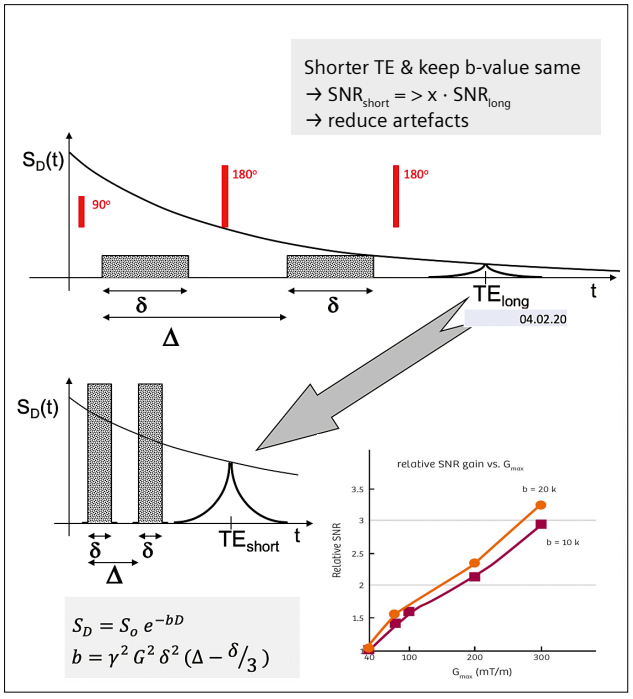

3 Diffusion imaging and its dependence on gradient performance.

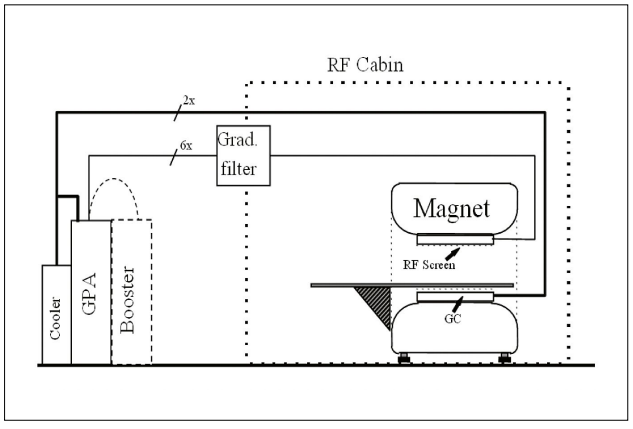

4 The MR gradient system.

The gradient system

The gradient system (Fig. 4) is composed of components generating the gradient field, including gradient coil and its driving power devices (gradient amplifier; and booster if available, as used in the early days of EPI); as well as connecting elements such as cables, gradient wall filters and cooling. The whole-body RF coil must also be considered, as eddy currents induced within its conductive elements may affect the quality of the gradient field, resulting in image quality degradation. Typically, gradient coils also house the shim system, which includes the space to place shim iron and a set of shim coils.

Let's now have a closer look at the two major components, the gradient power amplifier (GPA), sometimes also called gradient power supply (GPS), and the gradient coil (GC).

Gradient power amplifiers

From the very beginning of MR product development, Siemens kept the engineering and manufacturing of gradient amplifiers inside the company. The authors think that this was essential for the high performance of our gradient systems, as the integration of amplifier and coils requires close collaboration beyond just bit specs.

The purpose of a GPA is to supply the required voltage, V, and current, I, at a reasonable duty cycle, DC, (on/off ratio) to the gradient coil of inductance L and resistance R, according to

Equation 3

$$V(t) = R \cdot I(t) - L \frac{dI(t)}{dt}$$

For the very first MRI scanner generation, Siemens used linear high-precision music amplifiers. Their duty cycles are limited because the transistors are basically always on, and therefore experience excessive resistive losses.

Very early on, the Siemens Gradient Amplifier lab had focused on pulse-width modulated (PWM) amplifiers, and the first switch-mode GPA. The main advantage of a PWM amplifier is its high duty cycle (compared with linear amplifiers) as the transistors are being switched on and off only when needed, thereby minimizing resistive losses. It is quite impressive how PWM amplifiers perform compared to linear amplifiers. The latest Siemens Vida GPA performing at peak 2250 V and 1200 A built as a linear amplifier would have to face a total power dissipation of 3 x 2.7 MW = 8.1 MW, while realized as a PWM amplifier a transformer of 100 kVA (representing the total power dissipation for clinical and research scanning) is only required!

That is the reason why PWM amplifiers quickly became the standard for MRI gradient drivers, although they came with challenges due to switching noise and ripple, which

can reach up to the MR frequency and degrade MR image quality. More on this topic later.

The basic idea behind PWM amplifiers is that short voltage packages are switched to the gradient coil with frequencies up to 200 kHz (the switching frequency evolution of our GPAs is shown in Table 1). The voltage required to drive a certain slew rate, according to Equation 3, is supplied as described by the integral in Figure 5, as the average over many switching cycles with various on/off times. The semiconductors (switches) and the gradient inductance are configured in an H-bridge (Fig. 6). Each transistor T has an associated freewheel diode D [17]. Transistor T1 and T4 have D2 and D3 functioning as freewheel diodes, respectively; while T2 and T3 have D1 and D4.

With every new MR system platform, the latest reliable semiconductor technology was always used to build the best performing GPAs (Fig. 7).

The first generation, the Siemens MAGNETOM (internally called GBS I) with its linear amplifier, used 240 transistors in parallel in TO3 housing. The deionized water for cooling was at transistor potential. The performance was very meager, with peak values of 120 V and 150 A at a DC current of 30 A, meaning a duty cycle of 20%. A three-axis GPA required three full-sized cabinets (60 x 60 x 200 cm), one per gradient direction plus one for cooling (see Fig. 22B).

In 1987, this GPA was replaced with a PWM amplifier for the new MAGNETOM SP (GBS II) using stacked disk transistors which provided improved performance of 250 V and 160 A_{peak}, at a DC current of 80 A. The deionized water for cooling was still at transistor potential. All three gradient axes were now packaged into only one cabinet, a significant step forward in performance, space requirement, and costs. The drawback there was that the driver

Siemens MR system	Transistor switching frequency	Output ripple frequency
MAGNETOM (GBS II)	12.5 kHz	25 kHz
MAGNETOM Impact	25 kHz	50 kHz
MAGNETOM Vision	25 kHz	50 kHz
MAGNETOM Harmony & Symphony	50 kHz	100 kHz
MAGNETOMs with Cascade GPAs	20 kHz	200 kHz

Table 1: Switching frequency and residual output ripple frequency of Siemens gradient amplifiers.

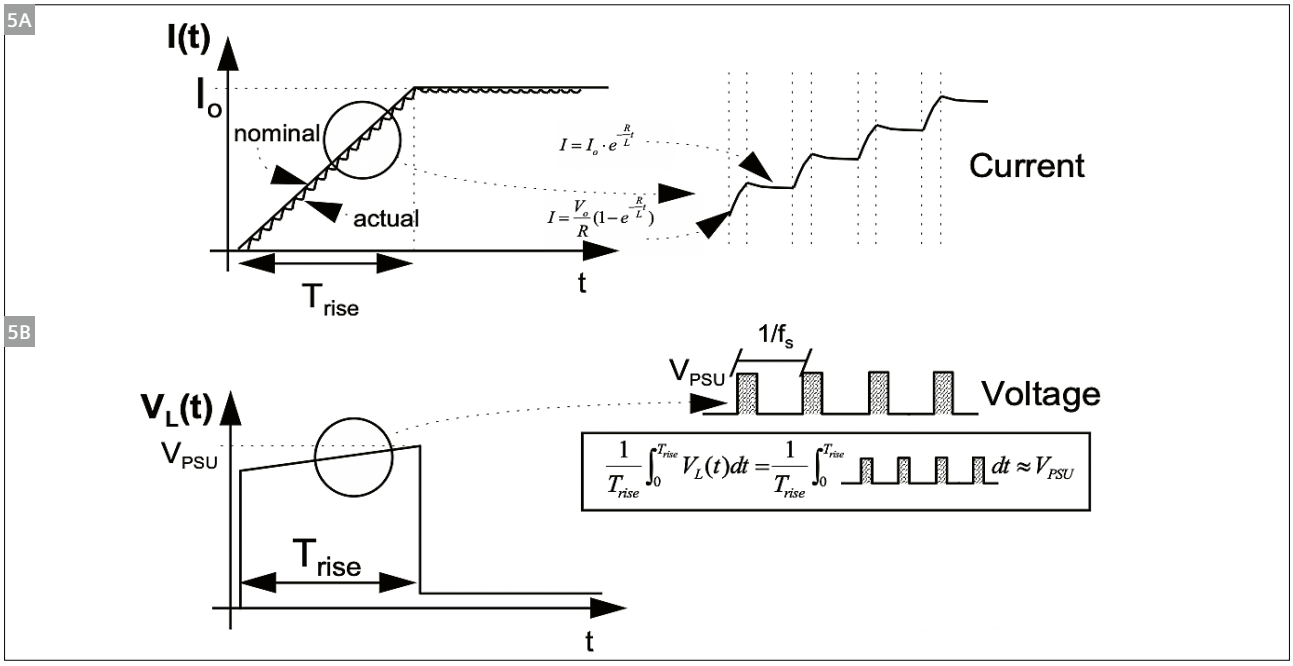

5 Principle of pulse-width modulated (PWM) amplifiers. **(5A)** Gradient current corresponding to a linear ramp (magnified version upper right). In reality these rise and falls are much smoother, and ripples cannot be seen in the current. **(5B)** Voltage required to perform the linear ramp, and integral conditions for the PWM voltage packages.

circuitry alone needed 200 W, due to the current-driven bipolar transistors. Today's MOSFETs and IGBTs are voltage driven, and need much less power.

A real leap in performance was made in 1991 with the introduction of MOSFETs (specifically BUZ325 transistors) for the MAGNETOM Impact [18]. With the circular design of the power stage, synchronous control was possible: Each semiconductor had the same driver signal transmission time and thermal conditions. Even this MOSFET was not perfect, as its intrinsic diodes had to be deactivated through tricky electric circuitry and external freewheel diodes. The digital gradient pulse form was transmitted via optical fibers, a first for Siemens and standard since then[2]. The power stages were air cooled but provided 300 V and 300 A_{peak}, resulting in a gradient strength of 10 mT/m for the first actively shielded gradient coil used in Siemens MRI systems (further information in the section on Gradient Coils). The Impact GPA was designed very conservatively with its circular arrangement. There was no prior knowledge on how to switch MOSFETs in parallel, as we used them as soon as they were available. Later, the peak amplitude was increased to 20 mT/m simply by changing some resistors in the control electronics, an easy upgrade for the installed machines. This caused some stir through the ranks at Siemens MR, as it seemed to be classical German over-engineering. Since then, every new system GPA had margins just big enough to handle local variations in electric power and slight increases in MR application demands, but not a 50% performance increase as happened with the MAGNETOM Impact.

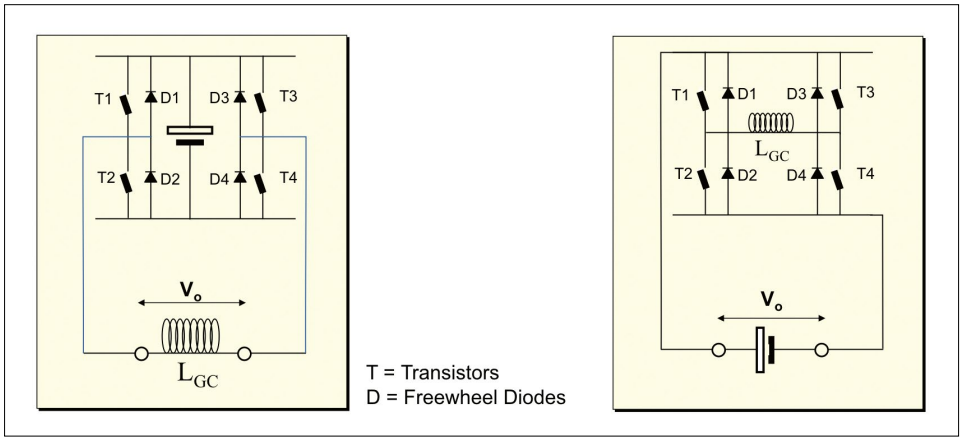

6 H-bridge configuration for PWM amplifiers. Both circuitry schemes are equivalent, but are shown because both are used in this paper.

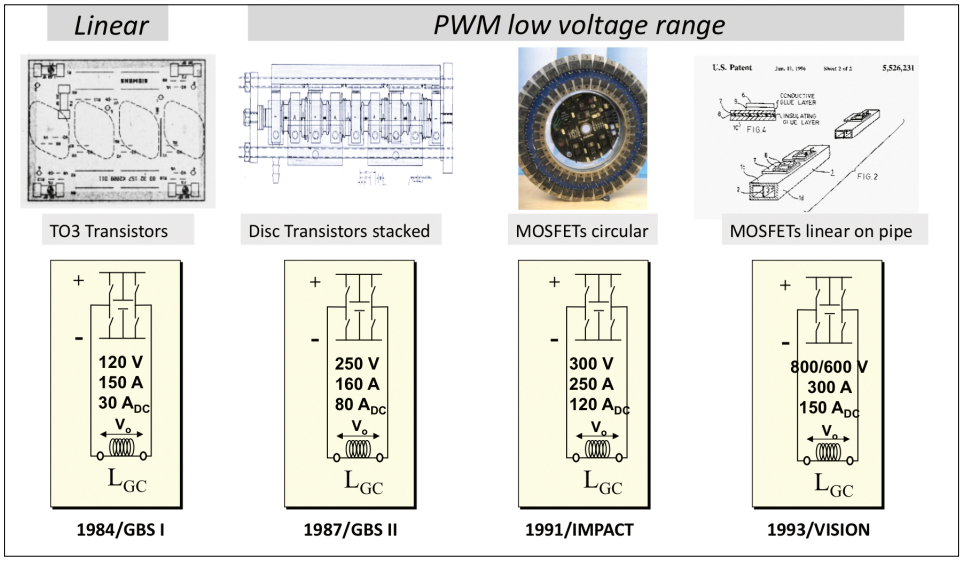

7 Single H-bridge PWM evolution at Siemens.

[2]*At about the same time Siemens started using direct current current transducers (DCCT) for measuring and controlling the output currents of the GPA. Günther Theil and Gunther Petzold convinced the Danish company Danfysik to integrate all necessary electronic components into one board with the current conductor to be probed running through the middle. Overall the precision for measuring the applied current in a gradient coil improved from 1% (as it is the case for classical music amplifiers) to ppm precision, which is essential for precise gradient pulses required for MRI.*

The next generation MRI was the MAGNETOM Vision in 1993. This also used MOSFETs, but as the ground plate was isolated from the cooling plate, it was water cooled again. Learning from the circular Impact design, we now used a rectangular pipe about 70 cm long. The cooling water was forced through that pipe. Each pipe had 36 transistors and 36 free-wheel diodes glued on and were all switched in parallel to achieve the peak current of 300 A. One such pipe resembled a half H-bridge. With its 600 V (originally 800 V, but more on this later) to drive the actively shielded gradient coil AS25, it reached 25 mT/m at SR 42 T/m/s. That design also had its challenges, and stabilizing it was quite a technological roller coaster. Nonetheless, the MAGNETOM Vision provided unique performance in the MR market. The peak amplitudes of 25 mT/m prepared the road towards EPI, but didn't reach the SR that would be required, yet.

Reaching the SR needed for EPI was an adventure that started in the late eighties at the Siemens Corporate research laboratory in Erlangen. When calculating the required gradient strength and switching speed, we concluded that at 2 Tesla, due to the short T2* of brain tissue, the total readout time for 128 x 128 EPI image should be no longer than 64 ms [19]. That required about 37 mT/m with a pure sinusoidal gradient pulse train to achieve a pixel size of about 2 mm. Sine gradient pulses were used as they could easily be achieved in a serial resonance circuit (Fig. 8). The capacitance C was tuned to match the inductance L of the gradient coil to reach a frequency of 1 kHz, according to

Equation 4

$$f = \frac{1}{2\pi} \cdot \frac{1}{\sqrt{LC}}$$

The capacitor was charged and discharged by cycling up and down, respectively (Fig. 8A). This is what we called "poor man's EPI", as it fixed the fast EPI RO to the X-axis. That up and down cycling caused parasitic times, which were avoided with the design shown in Figure 8B. Bipolar thyristor switches were switched in series and parallel to the capacitor, allowing to move the charge and discharge cycles outside the MR-relevant pulse sequence. By-passing the capacitor, any arbitrary gradient pulse-shape could be applied. Thyristors were precise enough to drive the rather slow 1 kHz RO pulses.

The next step was to move on to IGBT transistors [20] which in the meantime had become very powerful and far superior to thyristors. An H-bridge design was employed with the capacitor as dynamic voltage supply inside the bridge as shown in Fig. 8C. Figure 8E provides a look into the EPI booster box with its roll type capacitors. Karl-Heinz Ideler designed and build the first 3-axis EPI booster prototype [21] which was eventually installed at Beth Israel Hospital in Boston, MA, USA in 1992. Robert Edelman [22], Steve Warach, Paul Finn, Piotr Wielopolski [23] and others achieved landmark results beyond just using it for EPI-based imaging such as EPI-STAR [24] and diffusion imaging for stroke [25].

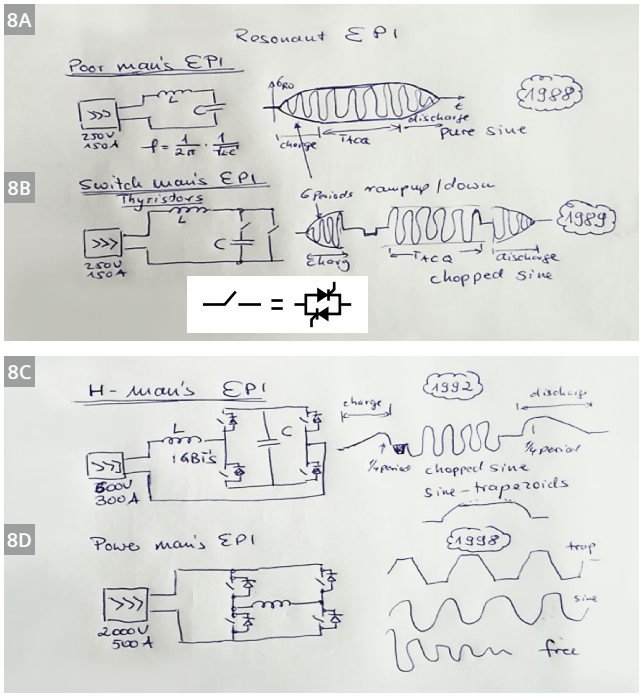

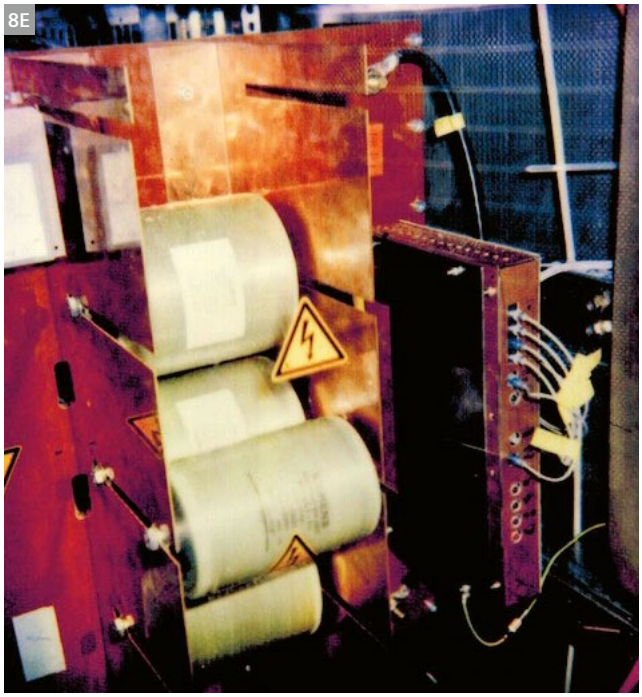

8 Left: The technological path of EPI at Siemens, from poor man's EPI to state-of-the-art. Right: A view into the booster box showing the capacitors for the resonance circuit.

Another group, the startup company Advanced NMR Systems was working independently on the challenge of EPI, under the direction of Richard Rzedzian and Ian Pykett, both trainees of Sir Peter Mansfield. While at first, ANMR intended to build their own imaging system, they instead contracted with General Electric to provide EPI capabilities as a retrofit to the Signa platform. In fact, their electronic solution to the problem of fast gradient switching was similar to (ours at) Siemens, using a series resonant circuit under tight control by IGBT transistors. ANMR chose to operate at a higher frequency of 1.4 kHz, thereby requiring proportionately higher peak gradient amplitudes. On the ANMR system, only the X and Y gradients could be used in echo planar mode. While this still allowed echo-planar imaging in all planes, it did not have the flexibility to switch phase and readout axes arbitrarily.

In its early phases ANMR partnered closely with the Massachusetts General Hospital NMR Center, collaborating with the applications team at ANMR, with the focus on diffusion and perfusion imaging [27]. The first ANMR "Instascan" product system was placed at the MGH-NMR center, where the first EPI based functional MRI, fMRI, experiments were performed. Jack Belleveau [28] and Ken Kwong [29] performed their seminal human BOLD experiments in 1991 with that EPI scanner.

When ANMR folded, its technology became the property of GE Medical Systems, who instead developed their own EPI booster technology [31] using inductive, as opposed to capacitive energy storage.

A similar resonant EPI booster was explored in Nottingham [30] at Sir Peter Mansfield's Lab, employing multiple serial resonance circuits to mimic a Fourier coefficient series.

Our resonant booster technology was eventually used for the MAGNETOM Vision, tuned to 833 Hz EPI (Echo Spacing = 600 µs), which brought EPI into the realm of clinical MR imaging. The 3-axis booster was housed in an extra cabinet, so all the gradient amplifier electronics were held in two cabinets (Fig. 4) and had no restrictions in use for conventional clinical MRI. Only the EPI application was restricted to sinusoidal ramps.

The MAGNETOM Vision system allowed to explore clinical stroke diagnostics using EPI diffusion imaging, and was also used in the now starting wave of fMRI research. Things moved on, however, with the MAGNETOM Harmony and MAGNETOM Symphony systems. More or less from scratch, we were able to develop a platform of components that could be integrated into different scanner types and field strengths.

For advancing GPA technology, we understood that performance needed to improve with output voltage and current, but the cost figure also needed to be improved.

A modular system was developed that allowed voltage stacking. The basic building block provided 400 V at 300 A_{peak}, so putting them in series provided 800 V, which doubled the SR. All 3-axis, including the 800 V upgrade, were packaged into one cabinet (Fig. 9, left). The base power module was still the pipe design we had used for the MAGNETOM Vision system.

As long as the MAGNETOM Vision existed as our EPI scanner, there was no need to increase the output voltage of this modular system to suffice for EPI. Yet sooner or later that challenge had to be tackled as by the end of the 90s MAGNETOM Vision was getting old and a new EPI capable MRI scanner needed to be developed. We had to face the challenge of how to continue: either boost the many-

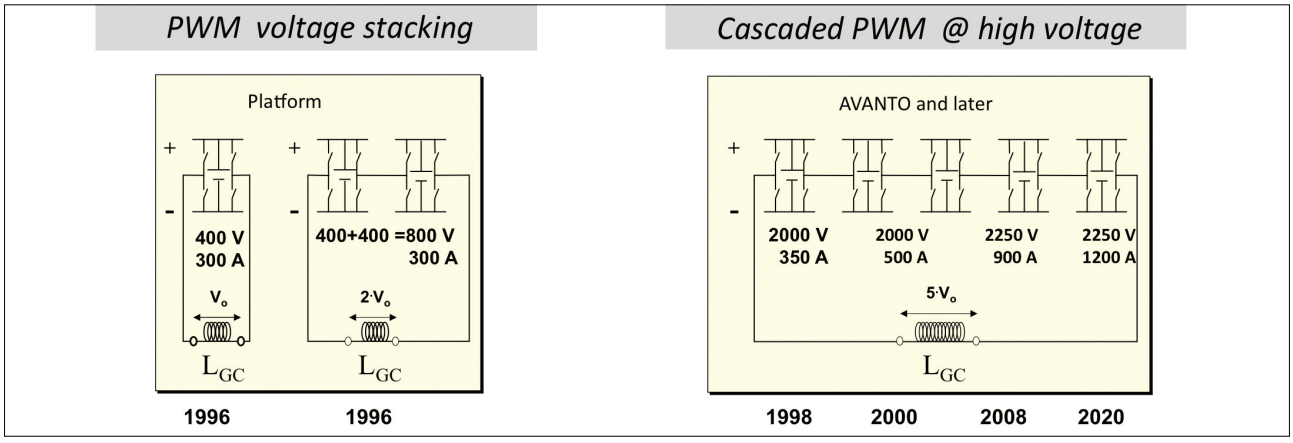

9 Voltage-stacked and cascaded PWM evolution at Siemens.

MOSFET technology that started with the Vision system (but without a booster), or find new more compact semiconductors such as IGBTs [32].

Stefan Nowak (one of the authors) spent 3 years at Siemens Semiconductors and saw the new IGBT module evolving. When returning to the MR R&D division in 1996, he focused on that technology. Two of us, Stefan Nowak and Franz Schmitt, still recall vividly the decisive experiment: the old but still very powerful many-MOSFET vs. the new IGBT modules. The later was humming away at significantly higher DC currents while the old overheated and went bust. A new era in GPA power electronics had come. The top right of Figure 9 shows the power electronics of half of an H-bridge of that new GPA.

With these platform GPAs, we could double the output voltage by adding another power stage (putting them in series; Fig. 9, left), while the switching frequency overall did not change. However, putting 5 power stages in series, as planned for the new GPA to reach 2000 V, would not be enough for high-performance imaging, and would have created challenges with RF spikes. Cascading [33], as we called it, helped to increase the switching frequency. The trick is that each H-bridge is time shifted by $1/5*1/f_s$, where f_s is the switching frequency of a single H-bridge. This gave five times the switching frequency of a single power stage at the output terminals. That allowed us to build very effective filters, as the inductances for such filter circuits decrease with increasing switching frequency, which reduced the size and resistive losses significantly. The new IGBT could handle much higher currents than MOSFETs. The series of cascade GPAs we have built over the years started at 350 A (throttled from 500 A) and has reached 1200 A, while the voltage has also increased to 5 x 450 V = 2250 V.

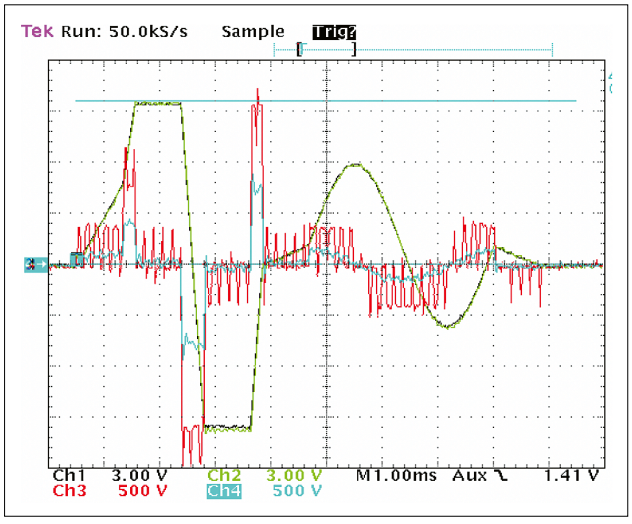

10 Oscilloscope trace: mixed trapezoidal and sinusoidal gradient pulse (green), unfiltered GPA output voltage (red), filtered output voltage (blue).

Figure 10 shows an oscilloscope trace, displaying the current and the unfiltered output voltage. The modulation of these H-bridges is cascaded until they reach the maximum voltage of 2000 V, i.e. when all stages (each supplying 400 V) are involved. Due to cascading switching frequency of 200 kHz at the output terminals is resulting.

It is remarkable to note that between 1983 and today the total power increase of several magnitudes was realized in one single cabinet.

Gradient coils

Gradient coil design also has changed significantly over the last decades. At the beginning, in MRI only Golay coils [34] were used, consisting of a continuous assembly of circular arc and straight-line conductors. However, they lacked good field linearity and efficiency. Further design steps were governed by a balance of computability and manufacturability, spiced with some imagination.

The next coil design employed polygons wrapped on a cylinder, connecting straight and curved conductors piece by piece (Fig. 11, bottom left). That offered more mechanical degrees of freedom to eliminate confounding higher orders in the field series.

At Siemens, these designs were first executed by Georg Frese, based on methods developed at the Erlangen Corporate Research lab (known in German as the "Forschungslabor") under Horst Siebold, Peter Henninger and Laxmikant Urankar in the "Feldkonfigurationen" team.

They had developed a mathematical library based on the Biot-Savart law, internally called the Urankar Routines. These routines provide the magnetic flux at any location in space generated by a piece of straight or arc segment wire carrying a unit current. The other tool developed here was MFB3D, used to evaluate a complete gradient coil design, calculating the magnetic flux B(r) inside the FOV. On top of these, the program called GOPT optimized the coil geometry automatically until specific goals such as field quality and field energy were achieved, under technical restrictions such as maximum coil length and diameter [35]. The z-component is of particular interest for MRI and is optimized to achieve the desired linearity. The transverse x and y components of the gradient magnetic flux, called Maxwell terms, unavoidable in nature are useless for MRI purposes, and are generally considered troublemakers as they contribute to eddy currents, PNS, can create imaging artifacts [37] and therefore also need to be considered when designing a gradient coil. In the early 80s, remote mainframe computers used for design calculation and optimization had a performance similar to today's smart watches, so you waited until the next morning for the result of a run – or for a short output saying "compiler error" because you had mistyped an O for a 0. For details on the mathematics see [36].

Unshielded designs were common in the early product lines. Siemens used them for the first two generations of the MAGNETOM systems. Internally these were called GBS I and GBS II, where GBS stands for Grund-Bau-Stein, loosely translating to basic building block, a modular concept that was seriously taken up later with the platform systems MAGNETOM Harmony and MAGNETOM Symphony. Commonality of components was essential to decrease the cost figure of an MRI scanner, so the same components could be used for different MAGNETOM systems and field strengths.

With the development of MAGNETOM Impact, actively shielded (AS) gradient coils were introduced at Siemens. This was driven by the 100% eddy-current overshoot needed for unshielded gradient coils, and by the growing pains of dealing with "incurable" higher-order eddy currents, generated by the outer fringe field of a gradient coil in the conductive environment, most prominently the cooling shields of the magnet and the cryostat wall. On the other hand, eddy currents in the RF screen could be cured by means of slotting it, as was explored during the development of EPI.

The idea of actively shielded gradient coils was invented around 1985 at the University Nottingham [38], the Massachusetts Institute of Technology [39] and General Electric [40] more or less simultaneously. Each axis of an actively shielded gradient coil is modelled as a primary (inner) and a secondary (outer) mesh layer (Fig. 12, right). Individual loop currents are optimized so that the required field quality, a linear gradient field, is achieved inside the FOV, while the magnetic flux outside the gradient coil at the location of the cryostat (for cylindrical superconducting magnets) is minimized (see Fig. 12) at the lowest possible inductance L. That prevents or at least minimizes the generation of eddy currents inside the cooling shields and cryostat,which is essential for good image quality in fast MRI.

The MAGNETOM Impact gradient coil, although shielded, was still based on the polygon train design. Primary and secondary coils were separated by blocks of wood and plastic formers and bandaged together (Fig. 13, left) into one unit. The space between primary and secondary coil was air filled. The coil could only be forced-air cooled. Water cooling was not yet necessary due to the low G_{max} and moderate duty cycle of the pulse sequences in these early days.

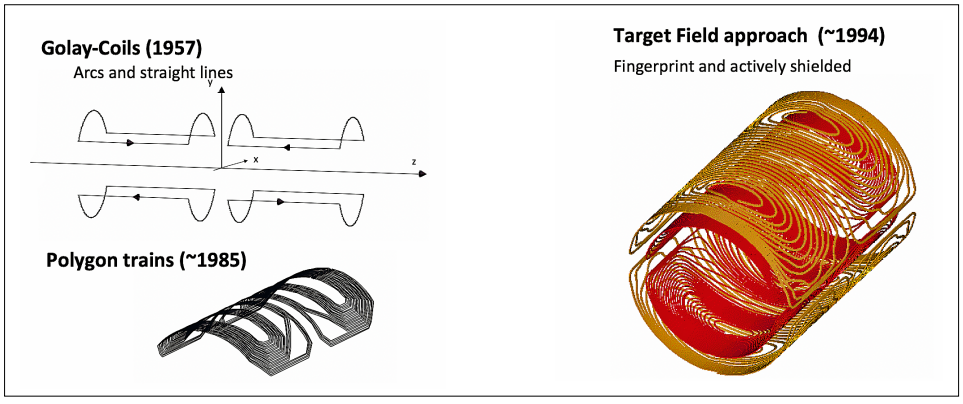

11 Winding design of a transverse gradient coil (Y). Upper left: Golay coil. Lower left: polygon design. Right: fingerprint design of an actively shielded y gradient.

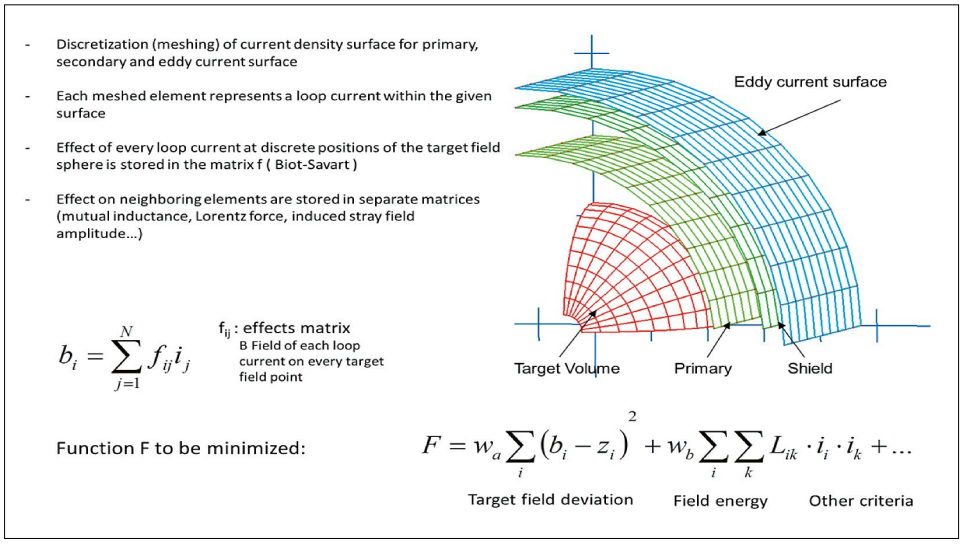

12 The current distribution in the primary and screen surface is calculated such that the required field quality is reached in the linearity volume, and the flux is minimized at the eddy current surface. Some numerical design principles and equations are shown.

From the EPI experiments performed at FL, we had learned that when driving a gradient coil with high voltages, extra measures must be taken to prevent the gradient coil from arcing and sparking (spiking as we called it; or white pixel noise according to GE). Voltage on our experimental EPI gradient systems was then already in the kV range. Due to the not perfectly filtered switching ripples of the gradient amplifier, RF spikes were making EPI almost impossible. EPI was geared towards cardiac imaging at that time, as it potentially allowed MR scaning of a beating heart. The first results were devastating, as the raw data were covered with bright pixels. These spikes rendered the image useless, unless you eradicated them from the raw data, which was a very tedious job that could take hours to produce a single decent image. This problem was solved with the next gradient coil, which we called Herz-EPI-II. It was still unshielded, but vacuum potting and using Litz wires cleared up the RF spikes, and allowed great EPI imaging [41]. This coil was high-voltage proof beyond 1 kV and was therefore an engineering target for the clinical product gradient coils to come.

Günther Pausch, a math and physics teacher, started working at Siemens in the gradient design group in 1984. He designed the MAGNETOM Impact gradient coil under the guidance of Georg Freese, exploring the field of numerical design methods. This eventually led to fingerprint designs, which are now state of the art. The numerical methods he developed, called target-field design, are still the basis of gradient coil design at Siemens – of course with significant improvements, for example to match general, complex geometric shapes, not only cylinders. The target-field design method can be seen as independent to the stream-function method developed at Peter Mansfield's lab in Nottingham by Robert Turner [42], which is an analytic method, while Günther Pausch's method is fully numerical.

The first realization of an efficient fingerprint design was the MAGNETOM Vision gradient coil, internally called AS25 (Fig. 13, right). New ways in building a gradient coil have been explored. As the Z gradient was directly wound on the cylindrical surface, transverse saddle shaped X and Y gradients, were laid out flat, fixed and then brought into a cylindrical shape by proper bending. The key person behind this technology development was Johan Schuster, who joined the MR business unit in the early 90s. This was also the first fully vacuum-potted product gradient coil, an adventure in itself. Setting up a manufacturing line for such a coil took special efforts. The first prototypes took 6 weeks from start to finish. When quality problems occurred – and they were plentiful in the beginning – it took quite some time to get them under control[3]. Eventually we managed to do so when Dietmar Lehne took control of the newly formed gradient factory, MRG. I (F.S.) joined MRG in 1994 to head the gradient and RF body coil design team.

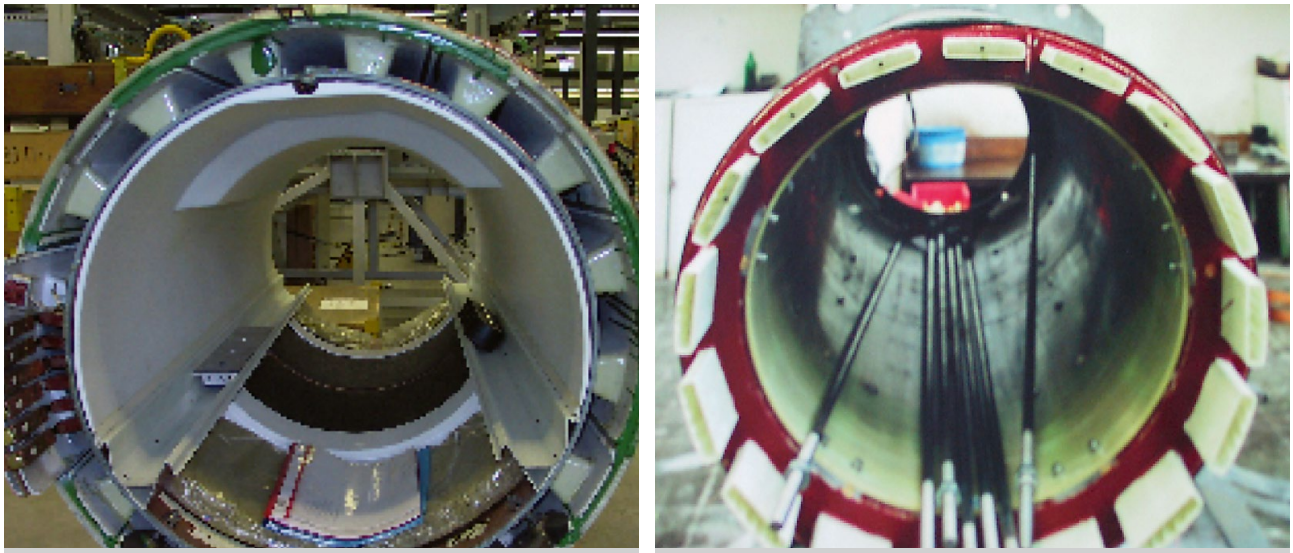

IMPACT VISION

13 MAGNETOM Impact gradient coil on the left, and fully potted MAGNETOM Vision gradient coil AS25 on the right. Note the use of the space between primary and secondary coils for placing the shim irons, the 16 rectangular pieces sticking out of the body of the coil, visible because this coil was still unfinished.

[3]An aspect we have experienced during the SARSCOV-2 outbreak: any measure being done to stop the outbreak took at least two weeks to see how the number of infected people changed and even four weeks and more to see how the number of deaths has changed. The logic is the same, i.e. you wait for 6 weeks to see if the changes on the make of the gradient coil has an effect on its quality build. Stay put and stick to the concept of clear thinking while you go through such challenging times.

The gradient factory consisted of the design teams for gradient coil magnetic field, the gradient power supply, and the RF body coil. The RF body coil was considered an integral part of the gradient coil, as its shield was directly attached to the gradient coil body. Also within MRG were the mechanical design team and the entire manufacturing line for gradient coils, gradient amplifiers, and RF body coils. The manufacturing line was about 4 km away from the offices of the design groups, which seems close when compared to the other MR vendors. When Siemens MR moved into the new facility at the Roethelheim Park in 2000, however, it brought us all very close together. The design teams on one side of the corridor, the manufacturing line on the other. A new era had begun. We think it is no exaggeration to say that this is the secret to the dominance of Siemens gradient performance.

MAGNETOM Vision used the first fully EPI-capable clinical whole-body gradient coil, which performed at 25 mT/m and up to SR 125 T/m/s in the EPI configuration using a resonant booster running at 833 Hz. This gradient coil weighed about 600 kg and was more than two meters long.

Already in the mid 90s, there was a desire to shorten the overall length of MR systems. This was then combined in the mid 2000s with a demand for bores wider than the usual 60 cm diameter, mainly to improve patient comfort and lower anxiety [43].

Large-scale GC manufacturing accelerated with the platform systems, when Manufacturing and R&D moved into the same building at the Roethelheim Park. Major investment in a modern vacuum potting system paid off quickly. We also had to learn how to test the quality of gradient coils. Partial-discharge measurement, previously used for large electrical transformers, was the key to this. It was applied to the MAGNETOM Vision gradient coil and is now an established part of quality assurance.

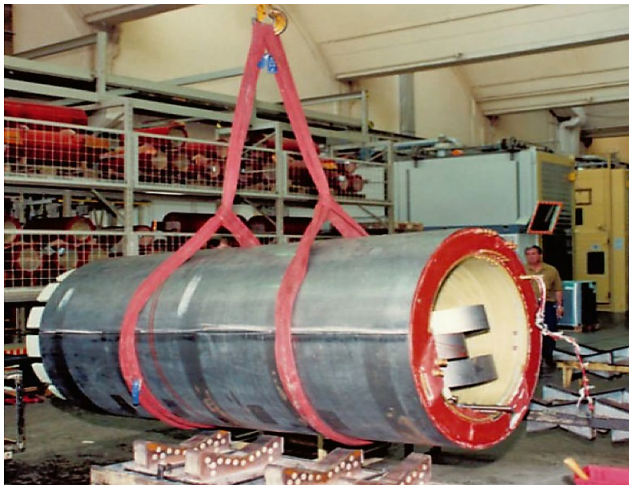

14 AS25 gradient coil right out of the potting chamber.

Head gradients

So far, we have described whole-body gradients. Now we turn to head gradient sets to highlight the Siemens activities in that field also. With dedicated head gradient insert coils, gradient performance can be increased substantially, as there is no practical physiological bound for amplitudes and SR.

Designing and building such coils goes back to the mid 90s, almost always driven by customer requests. We built our first head gradient coil, the HC40, in 1996, and delivered it to Mark Haacke's group at the Mallinckrodt Institute of Radiology in Saint Louis [44, 45]. The special feature of that coil was being directly cooled with deionized water through its hollow conductors which became again popular over the last 5 years [46]. That unshielded head gradient set reached 45 mT/m peak at SR 300 T/m/s. Due to its very low inductance, it needed an extra inductor in series with the gradient coil to match the overall inductance to the capabilities of the GPA regulator.

Another of our sets, the HC40seg, used segment coils [47] instead of saddle-shaped coils. We built and stacked segments with inner (primary) and outer (secondary) path to create the transverse gradients. That design was driven by the idea of minimizing acoustic noise. In the end, we did not follow it up, as a well shielded coil would have needed far too large a diameter, not a viable solution for the precious and restricted real estate inside the magnet.

For the 3T MAGNETOM Allegra, a head-only MR scanner, we designed the AC44 gradient coil which performed at 40 mT/m and SR 400 T/m/s. This coil was asymmetric in design to allow a shoulder cut-out for better positioning of the head in the sweet spot of the gradient coil and of the magnet [48]. The MAGNETOM Allegra was very popular in the neuroscience community since it provided the best EPI scanning available at that time, but it was not really suitable as a clinical machine for plain neuro scanning, as its FOV reached only two or three vertebrae bodies of the C-spine.

The asymmetric design continued with our unshielded AC88 head gradient line [49], which we used for our MAGNETOM Trio A Tim System. The coil was by intention unshielded, as the fringe fields in the cryostat and cooling shield of the 3T magnet were minimal due to large separation of gradient windings and cryostat. Eddy currents could be compensated by the classical method. This gradient system was conceived through discussion with the MGH Martinos Center, Van Wedeen, and Lawrence Wald, in particular. Its major focus was to increase G_{max} and decrease the echo time for DSI (see Figure 3). It used a special cradle system to wheel it in and out of the magnet (Fig. 15) and fitted inside the standard 600 mm patient bore without removing anything. It also used a huge mechanical switch (the Frankenstein switch as we called it) to switch between the clinical Trio gradient system and the experimental

AC88 system. The performance of G_{max} = 80 mT/m and SR 400 T/m/s was unique, and along with the Connectom gradient systems set the path for whole-body gradient system requirements to come.

For our 7T and 9.4T[4] research systems we used a redesigned MAGNETOM Avanto whole-body gradient coil (the Avanto-7T GC) which had beefed-up shim coil channels to match the required shimming needs at 7T. It gave 45 mT/m at SR 200 T/m/s. Some researchers considered it not fit for neuro imaging and fMRI at 7T. Therefore, we designed and built another fixed-mount asymmetric shielded head gradient set, the AC84, which fitted snugly into the bore of the Avanto-7T GC when the patient bore liner was removed. Its inner diameter was 400 mm and its outer diameter was 670 mm. With its 80 mT/m and SR 400 T/m/s, it matched the performance of the AC88. Kamil Ugurbil's group, at the University of Minnesota's Center for Magnetic Resonance Research, used that coil heavily, and exchanged it on a monthly basis with the Avanto-7T GC. That head gradient set was eventually abandoned when we built a better performing whole-body gradient coil, the SC72, for our UHF system. The bore size was chosen not to fit the AC84, as we were convinced that 70 mT/m at SR 200 T/m/s should be fine particularly for neuro imaging. That performance was possible by reducing the inner diameter (to 640 mm) and the linearity volume to avoid PNS. The reduction of the inner diameter of the gradient coil was possible as we saw no need for a whole-body RF coil for our UHF system – an assessment that still holds true today.

15 Handling of the insertable head gradient set AC88.

GE also demonstrated several head gradient systems for 1.5T [50] and for 3T systems as an introduction to the Connectom world [46].

Overall, head gradient systems allow unmatched performance for neuro imaging research purposes, but there is the limited use to brain imaging only, patient comfort, and the extra effort required to provide modern head RF coils that will fit in a head gradient coil.

Fight the heat

Gradient coils consist of current patterns in 3D space, usually in cylindrical layers. For a saddle coil, the current pattern can be water-jet cut into copper or aluminum sheets. Alternatively, wires (these may be block, filament or litz wires) can be laid out on a flat surface and fixed in place. Either of the conductors chosen is then bent over a cylindrical surface. Then, the layers and segments are connected to provide the desired gradient field.

The type of conductor material used is often a company secret. The questions are, what material offers the best performance with respect to power dissipation, including the skin effect due to driving frequencies beyond 1 kHz; and what material is best for manufacturing? Every conductor type experiences some ohmic losses and therefore produces heat. Minimizing these losses is key to high-performance gradients. Existing gradient system designs need electric line power of 50 kVA and more. This is quite a high number, since this heat must also be removed by the cooling system.

Conductor choice defines the heat generated in a coil. Figure 16 shows schematic impedance curves of four different wire types. As gradients are driven in a whole variety of pulsing schemes, the spectral bandwidth of gradient sequences is important. EPI is a perfect technology to demonstrate this, with an oscillating RO gradient in the region of 1 kHz. At this frequency, wire type 3 is clearly superior to type 2, which produces nearly twice as much heat.

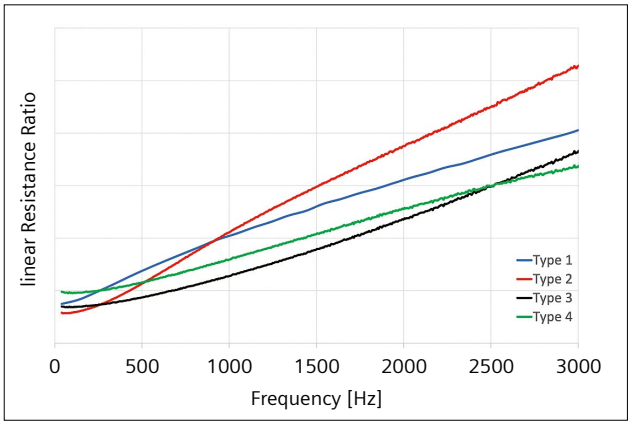

16 Impedance curves for 4 different wire types used in a gradient coil.

[4] *Work in progress: the application is currently under development and is not for sale in the U.S. and in other countries. Its future availability cannot be ensured.*

Hooking up a coil to scan human subjects

So far, we have described the development and manufacturing of the major gradient components at Siemens. When we hooked them up inside a magnet and entered the performance space of EPI, another adventure began.

Lorentz forces

A gradient coil experiences stresses caused by Lorentz forces

Equation 5

$$\underline{F} = q^* (\underline{v} \times \underline{B}_o)$$

with q being a charge (i.e, an electron) moving with speed $\underline{v}$ through the coil, and $\underline{B}_o$ the magnetic flux of the MR magnet. For saddle-shaped coils, there is typically a dominant banana-shaped bending mode (Fig. 17, top left, indicated by the force arrows). Here an unshielded gradient coil is shown. Actively shielded coils have the same bending modes, but internally the forces of the primary and the secondary layer oppose each other, and therefore create local compression and expansion also (Fig. 17, bottom left), which potentially can rip the coils apart if they are not properly potted. A variety of geometric modes are possible (Fig. 17, right). As Lorentz forces scale linearly with the magnetic field, it is obvious that gradient coil failures are more likely at high field. Entering the ultra-high-field world at 7T, we faced a learning curve that helped to improve the quality of coil manufacturing for the lower, clinical field strengths.

Vibration causes acoustic noise, so the higher the field, the higher the acoustic noise. Yet we have always managed to stay inside regulatory limits [51], even with our UHF systems.

Spikes

Early in the development of MAGNETOM Vision, Lorentz forces presented us with a nerve-wracking challenge. With the introduction of EPI, significantly higher currents and shorter pulses were applied, which led to friction of metallic and nonmetallic layers and caused charging and discharging. The poorly filtered switching ripples of the PWM power stages made this problem even more severe. While developing EPI at the Corporate Research lab we considered this period as very disturbing and somehow hopeless. I recall a time when due to the unfiltered switching ripple every metallic structure in and around the magnet was electrically charged up. Knocking on the RF cabin from the outside created an amazing blue sparking corona. That was eventually fixed by proper grounding and filtering the gradient power amplifiers better but did not solve all the troubles.

During testing of our first EPI prototype at the Beth Israel Hospital in Boston in early October 1992, I (F.S.) recall a time when the spikes were so devastating that EPI imaging was useless. After bringing in RF experts from the lab in Erlangen to help fix it, we gave up after a long week of tedious, yet unsuccessful work and decided to head to Cape Cod on Sunday instead. It was raining cats and dogs that weekend and humidity was significantly higher when we gave it a last try on Monday morning. Suddenly all the spikes were gone. The humid air suppressed electric

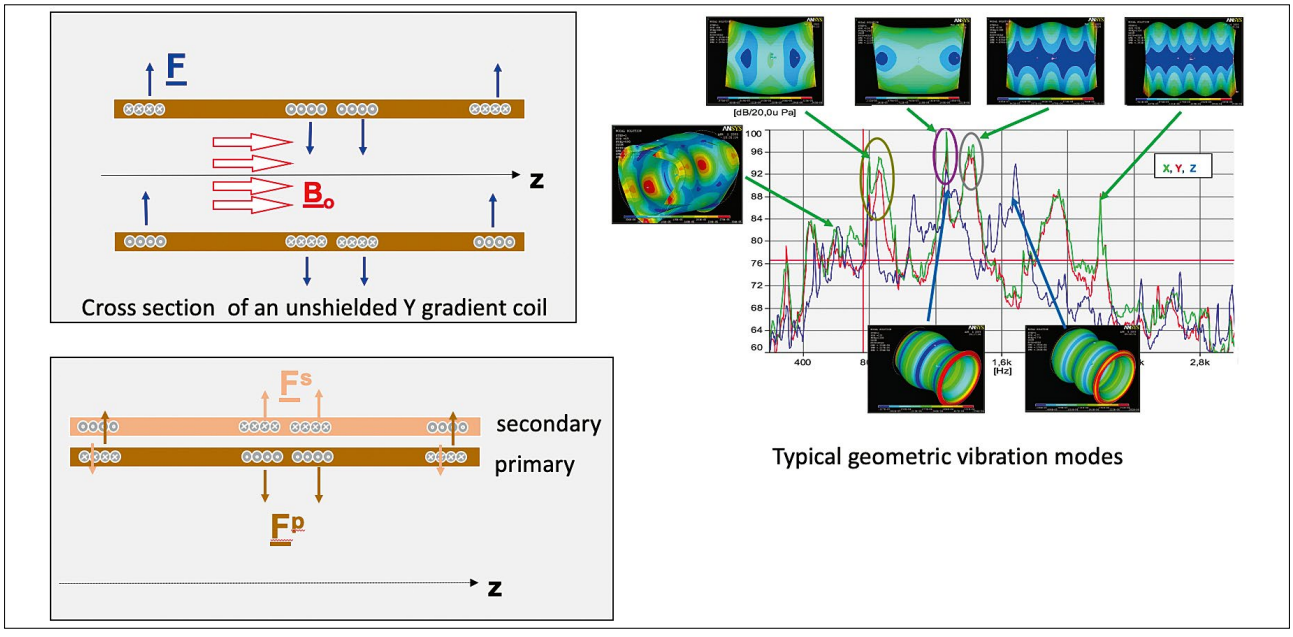

17 Lorentz forces and their effect on stresses and geometric modes of gradient coils.

discharges and therefore avoided spikes. This was one of those "aha" moments that lucky people sometimes have. A humidifier was brought into the RF cabin, and spikes were no longer a threatening issue – although they still pop up occasionally during the testing phases of early product prototypes.

When developing the Vision gradient system, we originally intended to start with 800 V PWM switching voltage. In the end it was not wise to continue with 800 V due to severe spiking. So we reduced the output voltage of the PWM stages to 600 V, which allowed us to fix the arcing and sparking. We eventually fixed the problem by cleaning up the materials inside the potted gradient coil, firmly grounding what needed to be grounded, properly galvanically seperating what needed to be insulated, and improving the mounting of the gradient coil inside the magnet. We also had to tackle air pockets inside the potted gradient coil. They are a major source of high electric field, as the permittivity ratio ϵ of epoxy to air is on the order of 4, and so increase the likelihood of arcs and sparks. A potpourri of spike trouble makers is shown in Figure 18.

Overall, this was the most challenging technological hurdle we have faced in our professional careers in MRI.

Coupling

Since the introduction of MAGNETOM Vision, Siemens gradient coils have electric shim coils as well as slots for placing ferromagnetic shim iron (Fig. 13, right). Shims are

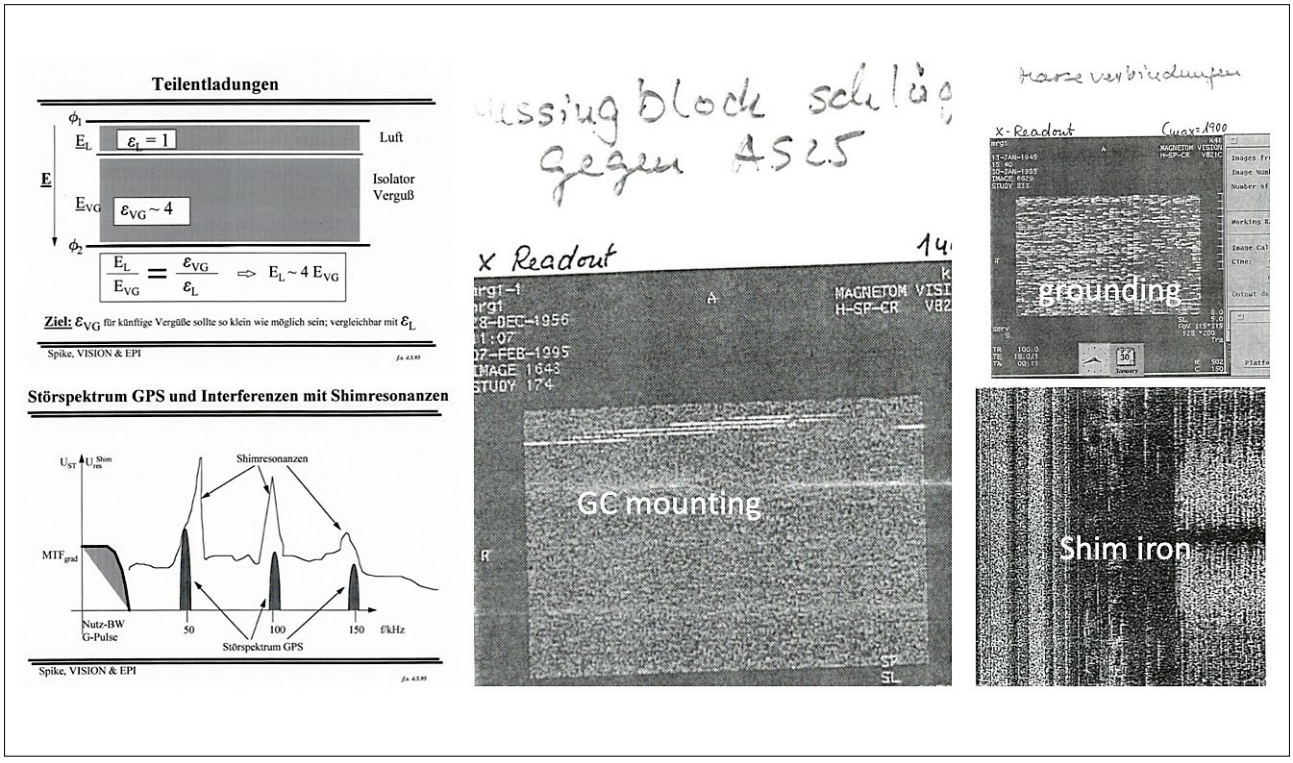

18 Spike phenomenas.

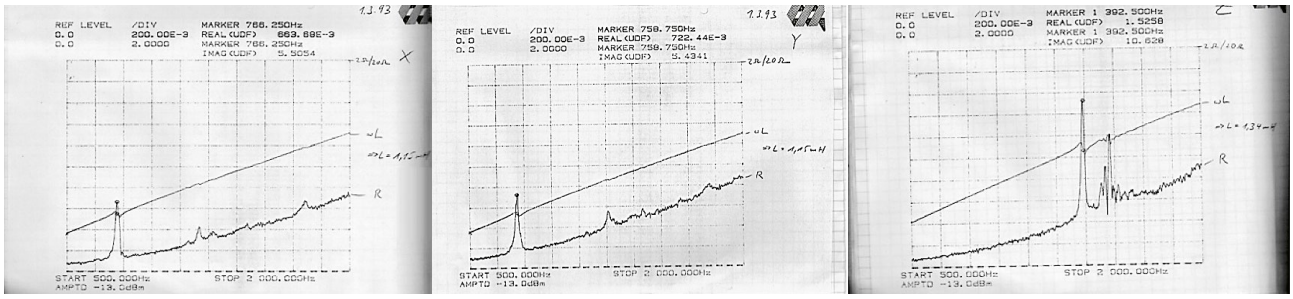

19 Effects of Lorentz forces on the impedance of a gradient coil. G_x, G_y, G_z from left to right. Transverse gradients (G_x & G_y) typically show resonance peaks at 700–800 Hz, depending on the diameter, wall thickness and length of the potted gradient coil, while for axial gradients (z-gradient shown on the right) the first dominant resonance is around 1400 Hz.

typically placed between the primary and the secondary layers, and so experience strong magnetic flux changes dB/dt. When the harmonics of GPA switching frequency coincide with resonances of a shim coil (A20 was the biggest trouble maker), arcing and sparking could occur at the shim coil terminals. Large filter networks helped on the Vision system. Later product generations solved this by decoupling the shim fields and reducing the switching ripples through output filtering at the GPA.

Electro magnetics-mechanics coupling into the shim iron itself was also possible. On our EPI prototype in Boston, the shim iron was attached to the magnet bore. Eddy currents could be induced even in the iron shim plates (some were about 10 x 25 cm) which vibrated and generated incredibly high acoustic noise levels (140 dB!), but only when one particular frequency was excited. That problem was solved by shrinking the shim plates and insulating each one from the others, and is no longer an issue.

Plotting impedance of the gradient coil against frequency reflects these mechanical resonances, where impedance can increase about 5-fold (Fig. 19). Each peak represents one of the bending modes shown in Figure 17. If I (F.S.) recall correctly, the shim iron peak was much broader (no screenshot exists from that unfortunately).

The electromagnetic-mechanical coupling described above is dependent on the magnetic field strength (Equation 5). Figure 20 shows impedance coupling results of a whole-body gradient coil and a head GC, spanning field ranges from 0 to 3T and 0 to 7T, respectively.

Driving an EPI RO gradient in such a peak frequency range could increase acoustic noise beyond legal limits, and also imaging would be degraded, as the GPA regulator (the feedback control system to assure that currents are correct) would be outside its normal range. In principle, this problem persists on modern systems, as vibration is unavoidable, but the total effect on image quality is very small, as todays GPA regulator compensates for it. However, the best remedy is to stay out of those vibration frequency bands to avoid excessive noise.

PNS

Our initial EPI experiments at the Siemens lab were performed on a head gradient system. Running EPI at 1 kHz and higher worked well, and no side effects were seen. As EPI was the only MR technique that appeared to allow single-shot imaging of a beating heart we run into another unexpected road block. The EPI RO at 1 kHz for a FOV of 400 mm required G_{max} on the order of 30 mT/m. I (F.S.) recall being the first subject of an EPI cardiac scan, and I experienced strong muscle contractions. I crawled out of the scanner while the EPI was still running and reported that unpleasant experience to my colleagues, who still thought I was in the scanner. We stopped any EPI activity while we tried to work out what was the root cause of these contractions. Soon we understood that due to a changing magnet flux, dB/dt, an electric field E is induced in the human body, and we had crossed a motor sensory threshold. To further understand this twitching phenome-

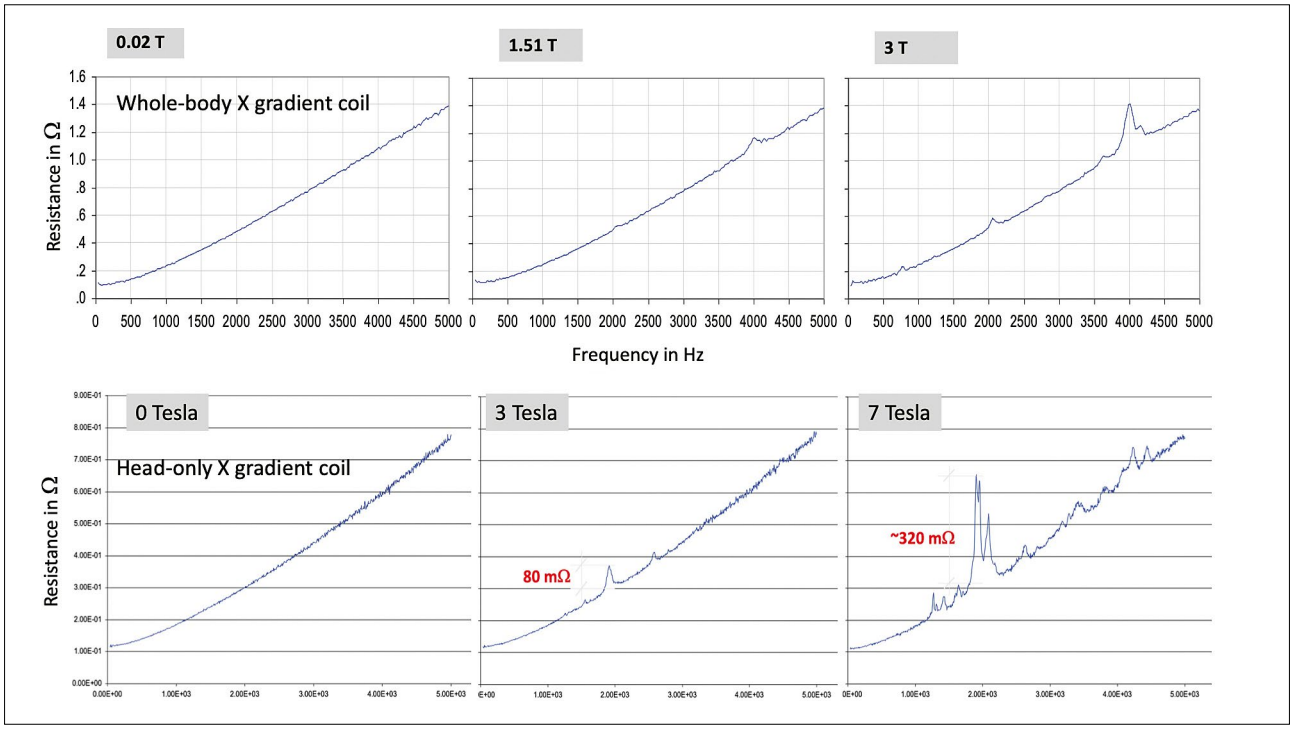

20 Resistance over frequency for head GC and whole-body GC for various magnetic field strengths.

non, we asked Tom Budinger, an MR pioneer from UC Berkeley, to help us explore the field of peripheral nerve stimulation (PNS).

Figure 21 shows some early experimental results from the Vision gradient coil, with a graph on the lower right showing all relevant physiological phenomena caused by dB/dt pulses. More details on this can be found in [10].

The results were published simultaneously with our main competitor, ANMR, at the RSNA 1989 [53, 54] and in 1991 in the Journal of Computed Tomography [55]. Nottingham University, where EPI was invented, later reported their view on PNS in 1993 [58], as did other groups in the U.S. who worked close with GE on that subject [56, 60].

In 1990, we performed animal experiments at UC Berkeley with Tom Budinger's group, equipped with a Siemens gradient system. The conclusion was that with MR gradients we could not induce any hazardous cardiac stimulation, such as extra heart beats or arrhythmia. We were at least a factor of 10 away from any cardiac risk.

Further explorations of PNS, together with Werner Irnich of the University of Giessen [57], eventually gave a clear picture of how EPI scanning and any fast switching gradient pulse sequences could be employed [59]. Based on that result, all product MRI scanners after the MAGNETOM Vision incorporated a PNS monitor (the SAFE monitor [62]), which would switch off the gradients when a certain threshold was exceeded, and also allowed look-ahead functionality.

The essence of all PNS experiments is that for EPI pulse trains (the worst case), be they trapezoidal or sinusoidal, there is a linear relationship between gradient rise time and gradient threshold amplitude (the amplitude at which the subject will feel muscle twitching). From a practical point of view, PNS is the limiting factor for fast switching gradients. In a whole-body environment, EPI can be comfortably deployed up to 40 mT/m at SR 200 T/m/s for x and z axis gradients. Faster switching is not permitted, and the PNS monitor will switch off the gradient. Higher gradient amplitudes are possible only with lower slew rates.

Summary

Since its clinical appearance, MRI underwent tremendous changes and improvements in applications from head to toe. This was mainly due to the numerous innovations and improvements in the MR system hardware. The RF system is considered the basis for the increased speed in MRI through parallel imaging (pRX) techniques such as SENSE and GRAPPA which allow in-plane speed up. Over the last 10 years Multiband (MB), and Simultaneous Multi-Slice (SMS) imaging has spread pRX techniques also across slices

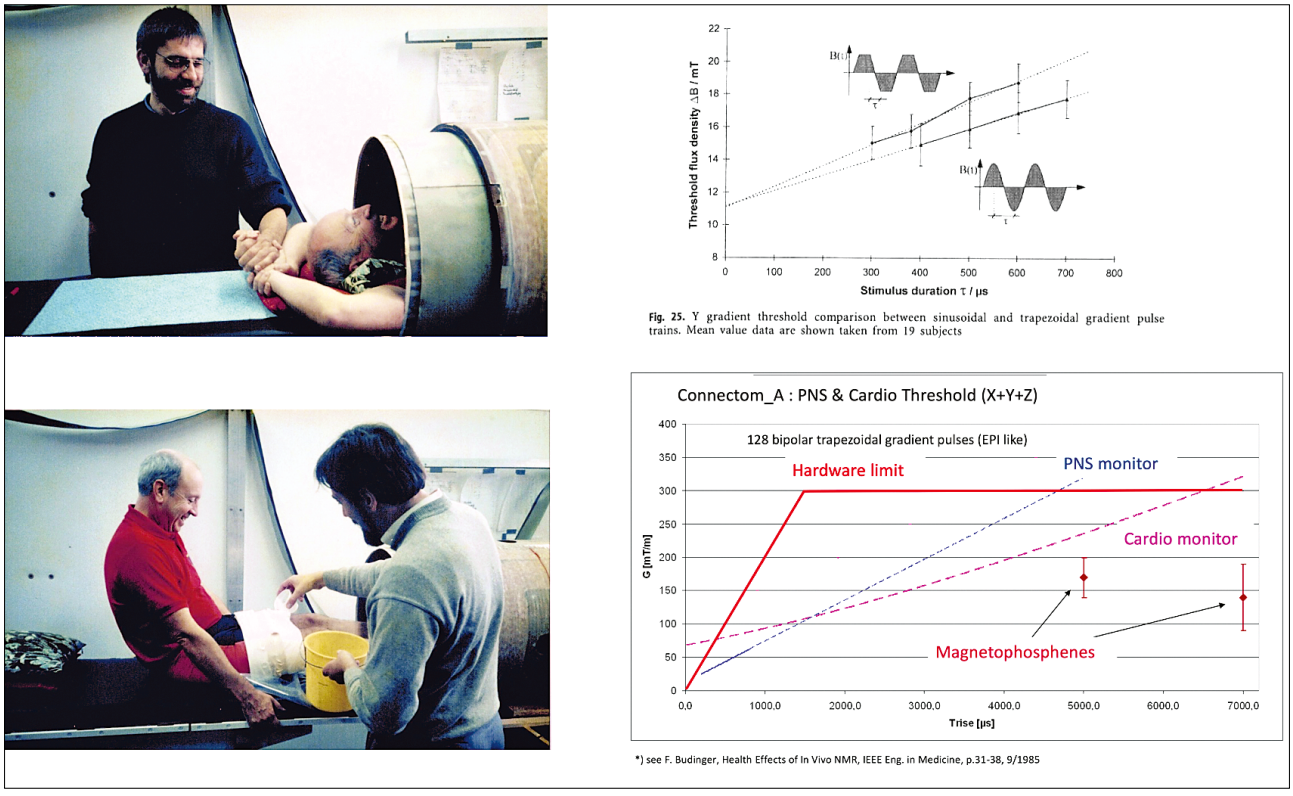

21 PNS experiments with an experimental gradient coil (MAGNETOM Vision) outside the magnet (left). The subject here is Tom Budinger. Top right shows PNS results on 19 subjects for sine and trapezoidal gradient pulses; vertical axis is B_{max} in units of mT. Lower right shows thresholds; gradient strength is shown in mT/m.

and allows 10fold and more speed up. Gradients on the other side also were essential to faster imaging. In particular EPI needs to be mentioned here. As a pure gradient echo technique the goal is to measure the entire heavily T2*-weighted FID in a time well below 100 ms. As EPI is SNR and PNS limited the gradient performance is limited to round about 40 mT/m at SR 200 T/m/s in whole-body settings. EPI is considered the work horse for fMRI research and is employed on hundreds if not thousands of human subjects per day around the globe. Combine EPI with diffusion weighting then we are rooted deeply in the clinical world for stroke and tumor diagnosis. For diffusion

22 **(22A)** Siemens Corporate Research "Feldkonfiguration" Team (~1984): Laxmikant Urankar, Peter Henniger, Horst Siebold.
(22B) GPA R&D team (~1984): from left to right: Harald Hofmann, Karl-Heinz Ideler, Gunther Petzold, Robert Bleisteiner, Stefan Nowak, Helmut Lenz, Günther Theil. In the background is the very first 3-axis gradient amplifier consisting of a total of 4 cabinets, one per gradient axis and one common cabinet for cooling.
(22C) GPA R&D team (~1983): from left to right: Helmut Lenz, Robert Bleisteiner, Stefan Nowak with a home build electrical model of a gradient coil to estimate the inductance of such coils. This was needed as at that time no whole-body gradient coil was existing for setting the PI regulator parameters of the gradient amplifier.
(22D) MR Physics including gradient coil design team (~1984): Jochen Abarth, Eckhardt Stetter, Franz Schmitt, Georg Frese, Angelika Mitzinek, Peter Heubes, Paul Margosian, Georg Ladwein, Paul Angstenberger, Günther Pausch, David Faul.
(22E) Gradient coil mechanical design team: Walter Derndinger, Tihomir Hudak, Christine Albert, Gerhard Nagengast, Günther Zebelein, Steffi Hammerl, Heinz Hahn, Elfriede Schönecker, Dietmar Lehne, Johann Baier.
(22F) GPA Electronics mechanical design team: Günther Pförtsch, Gernot Kwapil, Robert Zachmann, Karin Georgiatis, Bernd Räbiger, Klaus Albrecht, Norbert Hübler, Birgit Gmeinwieser, Karin Galster, Anne Kraus, Walter Rothmann, Peter Zöbelein.
(22G) Gradient coil design team (~2018): Peter Dietz, Stefan Stocker, Chris Ströhlein, Jörg Riegler, Andreas Krug, Sabrina Kreher-Harder, Martin. Sattler, Sascha Fath. Andrew Dewdney, Eva Eberlein, Anne Kraus, Simon Bauer, Axel vom Endt.
(22H) Connectom team (~2014): Herbert Thein, Johann Schuster, Franz Schmitt, Johannes Stadter, Eva Eberlein, Ralph Kimmlingen, Kevin Riedel. Helmut Lenz, who was very essential in getting the four GPAs synchronized should also be named here.

in clinical whole-body MRI systems we have now reached 80 mT/m gradient strength at SR 200. However, in the MR research world there seems to be no limit in requesting nearly unlimited gradient strength. We now have reached 300 mT/m in whole-body and head only set ups for targeted high-resolution neuro diffusion imaging. The Siemens Healthineers gradient development reflects that EPI route very nicely.

Acknowledgments

The authors would like to thank Horst Siebold, Georg Frese, Günther Pausch, Eckart Stetter, Robert Bleisteiner, Helmut Lenz, Mathias Blasche, Sascha Fath and Mark Cohen, UCLA, for their valuable support.

References

1 Oppelt A, Loeffler W. MAGNETOM Flash 2019;75(4):106-108.
2 Mansfield P. Multi-planar image formation using NMR spin echoes. J. Phys. C. 1977;10:L55-L58.
3 Moeller S, Yacoub E et al. MULTIBAND. Mag Res Med 2010;63(5):1144.
4 Setsompop K. Gagoski BA et al. Blipped-CAIPIRINHA for simultaneous multi-slice EPI with reduced g-factor penalty. Proceedings of the 18th Annual Meeting of ISMRM. 201018
5 Schmitt F, Arz W, Eberlein E et al. An ultra-high performance gradient system for cardiac and neuro MR Imaging. Proceedings of the ISMRM. 1999.
6 vom Endt A, Riegler J, Eberlein E et al. A High-Performance Head Gradient Coil for 7T Systems. Proceedings of the Joint Annual Meeting ISMRM-ESMRMB. 2007;15:451.
7 Kimmlingen R et al. Concept and realization of high strength gradients for the Human Connectome Project. Proceedings of the ISMRM. 2012;20:696.
8 http://www.humanconnectomeproject.org/
9 http://www.humanconnectome.org/
10 Kimmlingen R. Pioneers of Connectome Gradients. MAGNETOM Flash 2017 (68)2:122-136.
11 Blasche M. Whitepaper on Gradient Performance and Gradient Amplifier Power. Available at www.siemens.com/magnetom-world go to Publications > Whitepapers
12 Nagel AM, Laun FB, Weber M-A, Matthies C, Semmler W, Schad LR. Sodium MRI using a density-adapted 3D radial acquisition technique. MRM. 2009;(62)6:1565-1573
13 McRobbie DW. Occupational exposure in MR. Br J Radiology. 2012;85(1012):293-312.
14 Stejskal EO, Tanner JE. Spin diffusion measurements: Spin echoes in the presence of a time-dependent field gradient. J Chem Phys. 1965;42:288-92.
15 Tuch DS, Reese TG, Wiegell MR, Makris N, Belliveau JW, Wedeen VJ. High angular resolution diffusion imaging reveals intravoxel white matter fiber heterogeneity. Magn Reson Med. 2002;48:577-582.
16 Jin J. Electromagnetic Analysis and Design in Magnetic Resonance Imaging. 1998. ISBN 9780849396939.
17 https://www.elprocus.com/freewheeling-or-flyback-diode-circuit-working-functions/
18 https://en.wikipedia.org/wiki/MOSFET
19 Cohen MS, Schmitt F. Echo planar imaging before and after fMRI: A personal history. NeuroImage 2012;62(2):652-659.
20 https://en.wikipedia.org/wiki/Insulated-gate_bipolar_transistor
21 Ideler KH, Nowak S, Borth G, Hagen U, Hausmann R, Schmitt F. A resonant multi purpose gradient power switch for high performance imaging. Proceedings of the 11th Annual Scientific Meeting of the SMRM. 1992;11:4044.
22 Edelman RR et al. Qualitative mapping of cerebral blood flow and functional localization with echo-planar MR imaging and signal targeting with alternating frequency. Radiology. 1994;192:513-20.
23 Warach S, Gaa J, Siewert B, Wielopolski P, Edelman RR. Acute human stroke studied by whole brain echo planar diffusion-weighted magnetic resonance imaging. Annals of Neurology. 1995;37(2):234-241. https://doi.org/10.1002/ana.410370214
24 Edelman RR, Chen Q. EPI STAR MRI: Multislice mapping of cerebral blood flow. Magn Reson Med. 1998;(40)6:800-885.
25 Kolata G. New Brain Scanning Technique Can Show Strokes in Progress. New York Times. April 6, 1992.
26 Cohen MS, Weisskoff RM. Ultrafast MR Imaging. Magn Reson Imaging. 1991;9(1):1-37.
27 Rosen B, Belliveau J, Vevea J, Brady T. Perfusion imaging with NMR contrast agents. Magn Res Med. 1990;14(2):249-265.
28 Belliveau JW, Kennedy DN Jr, McKinstry RC, Buchbinder BR, Weisskoff RM, Cohen MS, Vevea JM, Brady TJ, Rosen BR. Functional mapping of the human visual cortex by magnetic resonance imaging. Science. 1991;254(5032):716-719.
29 Kwong, KK et al. Dynamic magnetic resonance imaging of human brain activity during primary sensory stimulation. Proc Natl Acad Sci USA. 1992;89(12):5675-5679.
30 Mansfield P, Harvey PR, Coxon RJ. Multi-mode resonant gradient coil circuit for ultra-high speed NMR imaging. Measurement Science and Technology. 1991;2(11).
31 Mueller OM, Roemer P, Park JN, Souza SP. A general purpose non-resonant gradient power system. Proceedings of the 10th Annual Scientific Meeting of the SMRM. 1991;10:130.
32 https://www.infineon.com/dgdl/Infineon-IGBT_or_MOSFET_Choose_Wisely-ART-v01_00-EN.pdf?fileId=5546d462533600a40153574048b73edc
33 Nowak et al. CASCADE IP ISMRM Syllabus
34 Golay MJE. Magnetic field control apparatus. US Patent 3515979A. Priority date 1957-11-04.
35 Frese G, Siebold H. Gradient coil system for a nuclear magnetic-resonance technique device. European Patent EP0073402B1. Priority date 1981-08-27.
36 Siebold H. A Computer Program for Optimizing Homogenous Field Magnets with Iron Yoke. IEEE Trans on Magn. 1988;24(1):408-410.
37 Bernstein MA, et al. Concomitant gradient terms in phase contrast MR: Analysis and correction. MRM. 1998;39(2):300-308.
38 Mansfield P, Chapman B, Turner R, Bowley R. Magnetic field screens. UK Patent GB2180943B. Priority date 1985-09-20.
39 Punchard W, Pillsbury RB. Magnetic resonance imaging systems. US Patent 4733189A. Priority date 1986-06-03.
40 Roemer P, Edelstein WA, Hickey J. Self-shielded gradient coils. Proceedings of the 5th Annual Meeting of the SMRM. 1986;(5):1067.
41 Schmitt F, Stehling MK, Ladebeck R, Fang M, Quaiyumi A, Bärschneider E, Huk W. Echo-planar imaging of the central nervous system at 1.0 T. JMRI. 1992;2:473-478.
42 Turner R. A target field approach to optimal coil design. J Phys D. 1986;19:L147
43 Heid O, Magnetic Resonance Imaging Magnet Assembly System with Improved Homogeneity. US Patent Application US20040178796A1.
44 Thompson MR, Kuppusamy K, Venkatesan R, Lin W, Haacke EM, Celik A. High resolution EPI imaging with a head gradient coil insert: applications to diffusion and functional MRI. Proceedings of the Fast MRI Workshop of the ISMRM. 1997:p181.

45 Tompson MR et al. Increased-Contrast, High-Spatial-Resolution, Diffusion-weighted, Spin-Echo, Echo-planar Imaging. Radiology. 1999;210:253-259.
46 Foo T, Lee SK, Tan ET, Mathieu J-B. Development of a Head-only Gradient Coil Prototype. GESIGNAPULSE.COM, Academic Issue 2015.
47 Zwanger MS, Porter D, Feiweier T, Reese T, Benner T, Kirsch JE. Compensation for Maxwell Cross-Terms in Diffusion-Weighted Imaging. Proceedings of the ISMRM. 2004;p101.
48 Meier C, Zwanger M, Feiweier T, Porter D. Concomitant Field Terms for Asymmetric Gradient Coils: Consequences for Diffusion, Flow, and Echo-Planar Imaging. Magnetic Resonance in Medicine. 2008;60:128-134.
49 Kimmlingen R, et al. An easy to exchange high performance head gradient insert for a 3T whole-body MRI system: first results. Proceedings of the ISMRM. 2004;p1630.
50 Alejski A, Chen Y, Rutt BK. Ultra-high-resolution Imaging with a clinical MRI. IEE Instrumentation & Measurement Magazine. 2002;5(2):18-22.
51 Foo T, Lee S-K, Tan ET, Mathieu J-B. Development of a Head-only Gradient Coil Prototype. GESIGNAPULSE.COM Academic Issue Spring 2015;11-15.
52 NEMA MS 4-2010: Acoustic Noise Measurement Procedure for Diagnostic Magnetic Resonance Imaging (MRI) Devices.
53 Goldfarb JW, Schmitt F. A robust method to remove spike artifacts through HPF post-processing. Book of abstracts ISMRM. 1996;3:1646
54 Cohen MS, Weisskopf RM, Kantor ML. Evidence of peripheral stimulation by time-varying magnetic fields. Proceedings of RSNA. 1989;75:1188.
55 Fischer et al. Physiological effects by fast oscillating field gradients. Proceedings of RSNA. 1989;75:1189.
56 Budinger TF, Fischer H, Hentschel D, Reinfelder H-E, Schmitt F. Physiological effects of fast oscillating magnetic flux gradients. J Comp Ass Tomog. 1991;15:909-914.
57 Reilly JP. Electrical Stimulation and Electro-pathology. Cambridge University Press, Cambridge-New-York-Oakleigh. 1992.
58 Irnich W. Magnetostimulation in MRI. Magn.Reson.Med. 1995;33(5):619-23.
59 Mansfield P, Harvey P. Limits of neural stimulation in echo-planar imaging. MRM. 1993;29:746-758
60 Schmitt F, Wielopolski P, Fischer H, Edelman RR. Peripheral Stimulations and their Relation to Gradient Pulse Shapes. Proceedings of the SMRM. 1994;p102.
61 Schaefer DJ, Bourland DJ, Nyenhuis JA, Foster KS, Licato PE, Geddes LA. Effects of simultaneous gradient combinations on human peripheral nerve stimulation thresholds. Proceedings of the Society of Magnetic Resonance. 1995 (Vol. 1220).
62 Hebrank F, Gebhardt M. SAFE model – a new method for predicting peripheral nerve stimulation in MRI. In Proceedings of the 8th Annual Meeting of ISMRM, Denver, CO, 2000. p. 2007.

About the Authors

All three authors have been hired in the beginning of the MR product development.

Eva Eberlein, a physicist, started in 1986 in the gradient design team. Eva first focused on shim coil optimization (part of the gradient coil assembly) as well as the shim measurement tool. She later focused on designing gradient coils. Today she is heading the gradient coil design team.

Stefan Nowak, an electrical engineer, started in 1982 as an intern and later for his Diploma thesis in Electrical Engineering (actually RF engineering!) on building a GPA prototype to become the first product gradient amplifier. When finished with his thesis he joined Siemens in 1984. With some years off the MR gradient amplifier electronics development to work at Siemens Semiconductors on high power semiconductors (1990–1993). He then worked as a consultant for MR to develop the product EPI booster. In 1995 he joined MR again as an engineer in the GPA electronics lab and was transferred to the healthcare central component factory, CO. Stefan headed the GPA design group until 2015 and at the end of his career worked at Siemens Corporate Research.

Franz Schmitt, a physicist, started in 1983 to work in the physics group of Wilfried Loeffler and Eckhardt Stetter playing with the first experimental MR scanner (0.1T open resistive magnet) in the so-called “Spanienhalle”, learning from Peter Heubes in particular what MR-technology means, do trouble shooting and how to get it running. His first closer contact with gradients started when he worked on developing methods to measure the gradient modulation transfer function. Later he focussed on hardware and physics of faster MR imaging, culminating in the development of Echo-Planar Imaging, EPI, at the Siemens Corporate Research Lab, together with Hubertus Fischer, Helmut Barfuss, Dietmar Hentschel, Ralf Ladebeck and Erich Reinfelder under the leadership of Arnulf Oppelt. This is when Stefan and Franz joint forces from 1989 on to fulfill the EPI gradient power demands. From 1994 until 1999 Franz was in charge of the gradient development. After spending 4 years at the MGH Martinos Center in Charlestown, MA to learn about neuro imaging he returned to be the head of the gradient manufacturing until 2006 and then also headed the gradient design team again until 2008 before diving into MR collaboration and Ultra High Field until he retired in 2014. In every of these steps, gradients always have been a core of his activities.

Contact

Franz Schmitt
schmittfranz53@gmail.com

Eva Eberlein
Eva.Eberlein@Siemens-Healthineers.com

Stefan Nowak
stfrno@gmx.de

Pioneers of Connectome Gradients

Ralph Kimmlingen

Siemens Healthineers, HC DI MR TR R&D-PL, Erlangen, Germany

Reprinted from MAGNETOM Flash (68) 2/2017

Abstract

A typical human brain contains 100 billion neurons which have about 10,000 individual connections with their neighbors. Being able to map structural and functional connectivity of an individual brain could be a first step on a new way of understanding and diagnosing mental illnesses. Continuous improvements on noninvasive magnetic resonance imaging (MRI) methods like functional MRI, resting-state MRI, and diffusion MRI enable this information (connectomics) to be obtained for the first time on a large human databasis. A key parameter is the available gradient field strength for diffusion-sensitive MRI sequences [1–3]. Siemens MR has developed two powerful prototype gradient systems for this purpose, which have been employed at five different locations in the US and Europe since 2011 (Fig. 1).

Up to today, the nervous system circuit diagram ('Connectome') of few creatures is known. Back in the early 1980s the little roundworm called C. elegans was discovered to have a nervous system of roughly 300 neurons showing a total of about 7,000 connections [4, 5]. Using invasive anatomical and neural-tracing techniques, mammalian brains like that of mice or primates are still under investigation. These methods are capable of an in-plane resolution of 40 µm [6, 7].

New non-invasive imaging methods which enable the study of brain connectivity of living humans have been developed since the beginning of this century. They are known as MR Imaging of anisotropic diffusion of water in the brain, and resting state fMRI [8–10]. The related advances in imaging technologies and data evaluation are empowering us today to study the human brain as an entire organ.

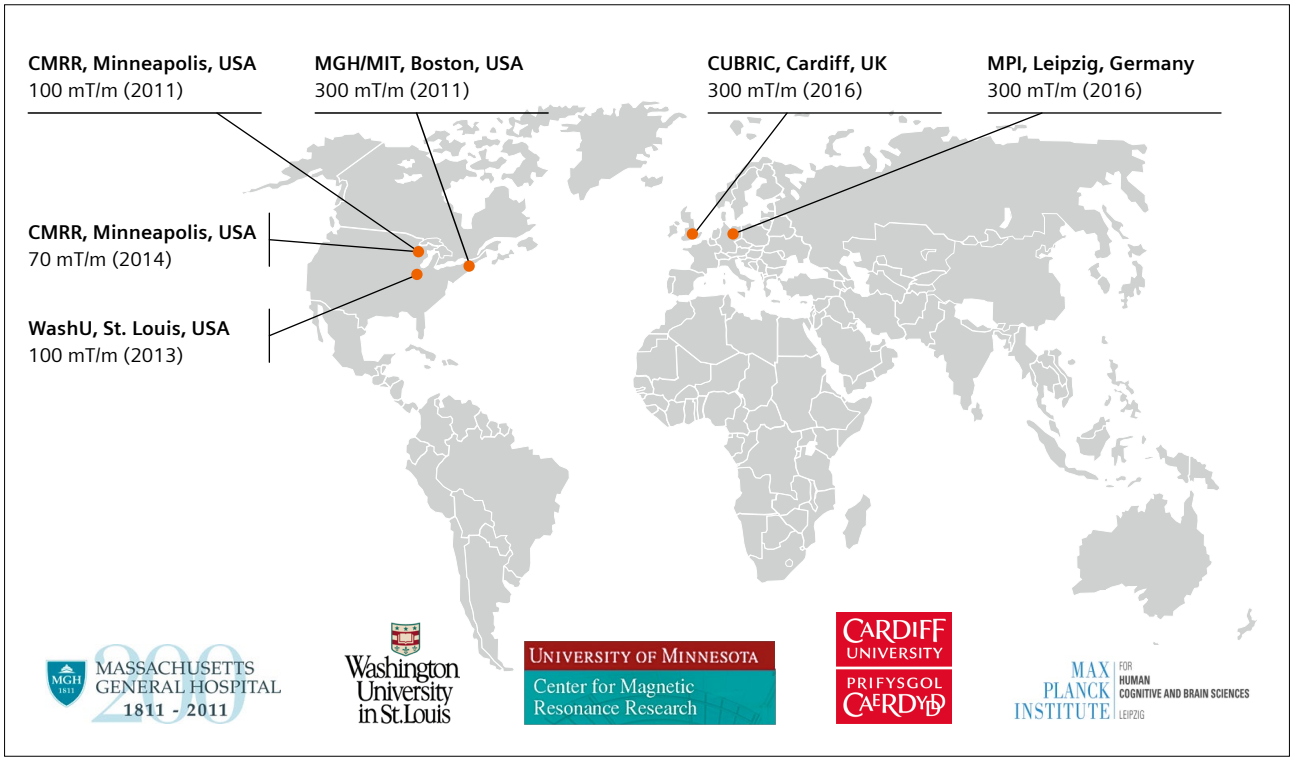

1 MAGNETOM Connectom scanners by Siemens Healthcare have been employed at five different locations since 2011.

A group known as 'Blueprint for Neuroscience Research', a collaboration among 15 National Institutes of Health (NIH) in Bethesda, Maryland, USA, decided in 2009 to fund a five-year initiative for mapping the brain's long-distance communications network. The goal of the so called Human Connectome Project (HCP) was set to construct a map of the structural and functional neural connections *in vivo* within and across individuals. The HCP was funded with $40 million and comprised two research efforts: the first, a five-year project at the Center for Magnetic Resonance Research (CMRR) in Minneapolis, Minnesota, in collaboration with Washington University, St. Louis, Missouri, and the second a 3-year project at the Massa-chusetts General Hospital's (MGH) Martinos Center in cooperation with the University of California, Los Angeles. A comprehensive description for the HCP can be found in a 2012 Nature article [11].

In order to map the human connectomics, the Washington University & the University of Minnesota (WashU-Minn) consortium, utilized resting state fMRI and high angular resolution diffusion imaging (HARDI) – a special diffusion imaging technique. However, Diffusion Spectrum Imaging (DSI) – a general form of Diffusion Tensor Imaging that was pioneered in 2005 at the Massachusetts General Hospital (MGH) – was the method of choice for the MGH/University of California at Los Angeles (UCLA) consortium. To pursue this challenging task, both of these consortiums approached Siemens Healthineers to propose working together in hardware technology, more specifically in special gradient systems, which will enable the demanding diffusion imaging.

More recently, two European research centers have joined the exclusive club of Connectome gradient users. In 2016, the Cardiff University Brain Research Imaging Centre (CUBRIC), equipped with a 300 mT/m MAGNETOM Connectom, two 3T MAGNETOM Prisma and a MAGNETOM 7T system1, was inaugurated by Queen Elizabeth II. At the end of 2016, the Max Planck Institute for Human Cognitive and Brain Sciences, Leipzig, Germany, also installed a MAGNETOM Connectom 3T MRI system[1].

Gradient technology

Siemens Healthcare introduced the first MAGNETOM 0.35T whole-body scanner in 1983 and has continuously extended the product portfolio with higher magnet and gradient field strengths. Starting with a peak amplitude (G_{max}) of 3 milli-Tesla per meter (mT/m) and a slew rate (SR) of 2 T/m/s in the early 1980s, today's (2017) clinical high-end 3T scanner MAGNETOM Prisma achieves a G_{max} of

[1] *MAGNETOM Connectom and MAGNETOM 7T is ongoing research. All data shown are acquired using a non-commercial system under institutional review board permission. Siemens does not intend to commercialize the system.*

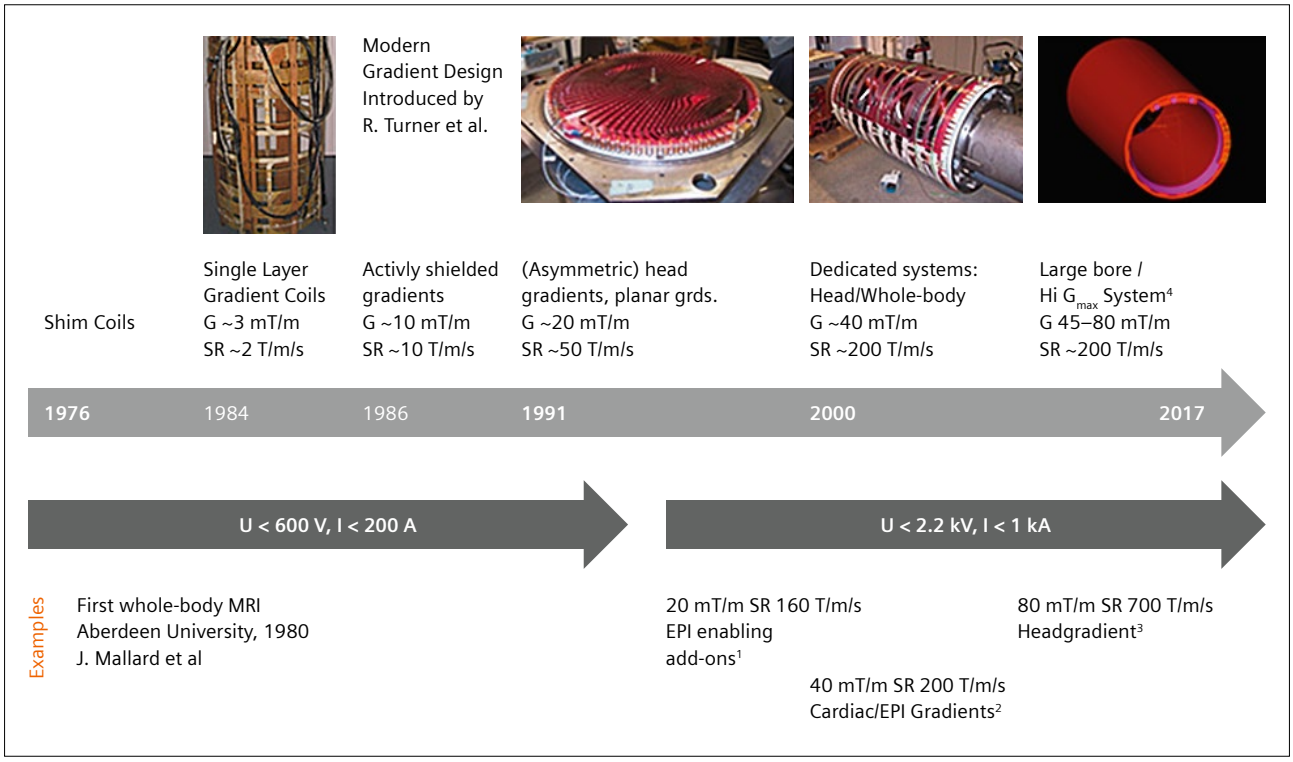

2 Gradient history of MRI systems.
[1]Cohen MS, Weisskoff RM. MRM. 1991; [2]Schmitt F, Eberlein E. et al. ISMRM, 1999; [3]Vom Endt A et al. ISMRM, 2006;
[4]Equals an increase of gradient power (slewrate x amplitude) of three magnitudes over 20 years.

80 mT/m and a SR of 200 T/m/s (see Fig. 2). Gradient system performance depends on many opposing factors including G_{max}, SR, linearity volume (LV) and available patient bore diameter. Highest performance demands are created by diffusion-weighted sequences which expect fast gradient switching for the readout pulses, highest peak amplitude / duty cycle for the diffusion pulses, and excellent shielding of eddy fields. As a consequence, gradient coils optimized for whole-body applications with a large linearity volume and inductance require high-voltage/-current power supplies. Starting with the first applications of the EPI imaging method in the early 1990s [12], especially gradient slew rate became a challenge for gradient system design. First attempts to reduce the rise time of EPI readout gradients involved additional resonant circuits, so-called 'EPI boosters' [13, 14].

With conventional gradient design methods [15, 16], SR increase (at otherwise constant parameters) can be

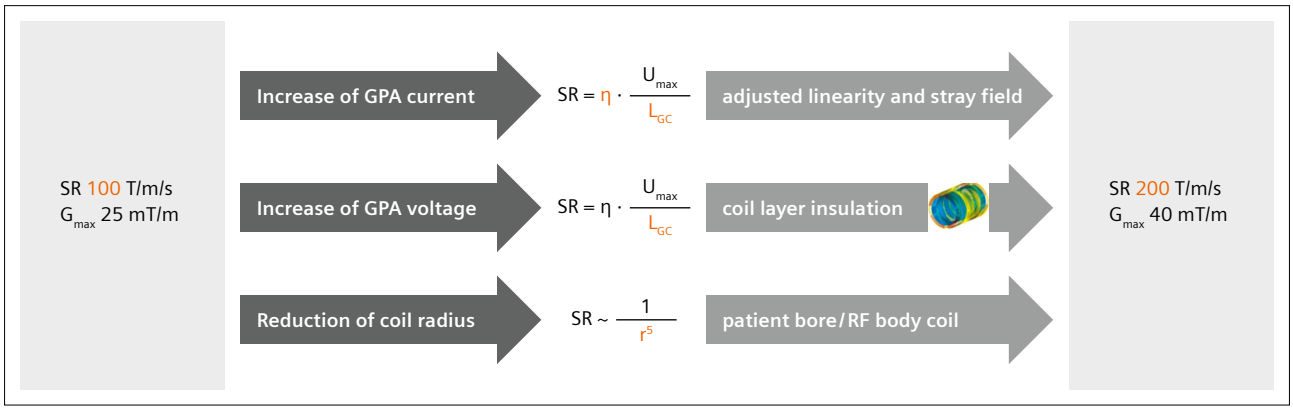

3 Improved gradient performance parameters (maximum gradient amplitude (G_{max}) or slew rate (SR)) can be achieved by either increasing gradient amplifier (GPA) power (via maximum voltage U_{max}) and adjusting the coil design (via field efficiency (η) or inductance (L_{GC})) or by a reduction of the coil radius (r) and adjustments to the RF body coil and/or the patient bore diameter.

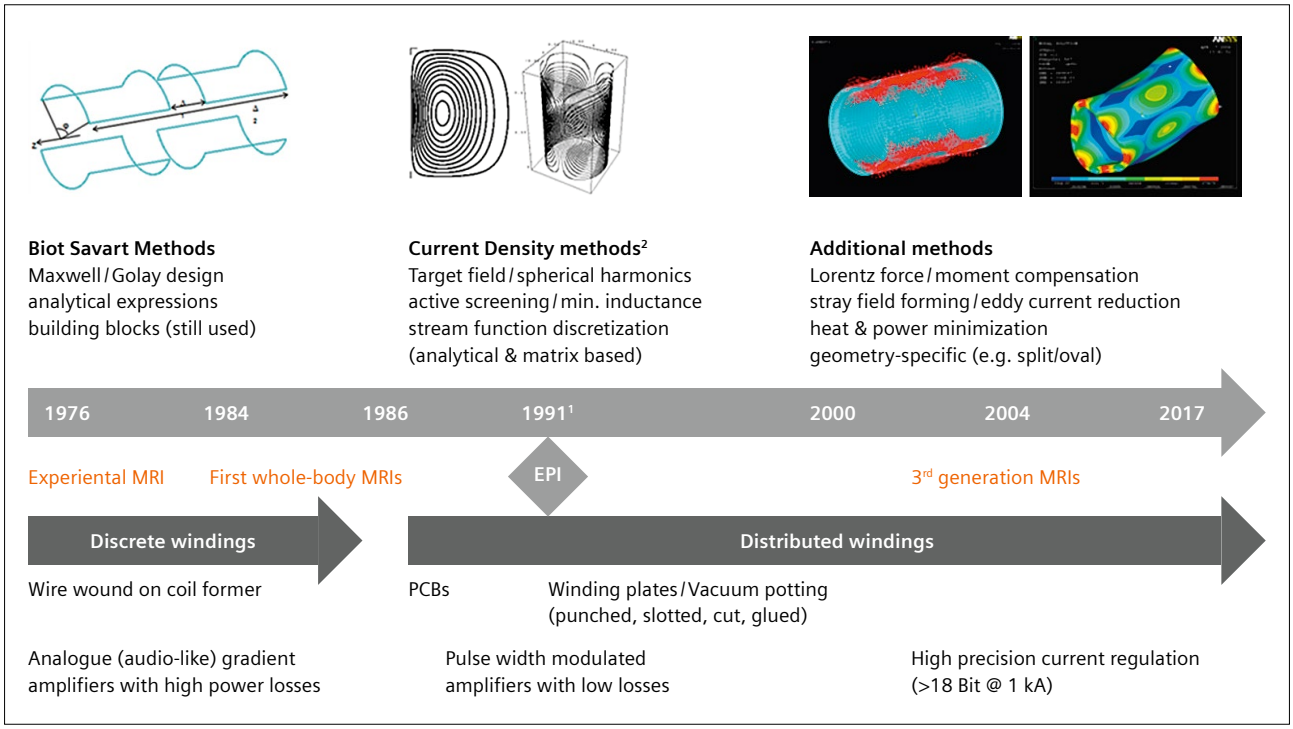

4 History of gradient coil design methods.
[1]In 1991, PNS (peripheral nerve stimulation) proves to limit gradient performance (predicted by T. Budinger 1979);
[2]R. Turner, Gradient Coil Design, A Review of Methods, MRM 11:903 (1993)

achieved by either increasing the voltage of the power amplifier (GPA) or by reducing the inductance of the coil. Besides using more than a single amplifier and coil-set [17], the third alternative for higher SR is to reduce the inner radius of the coil system (Fig. 3). The strong (5^{th} order) dependence of the SR from the coil radius leads to about a factor of two increase when changing from 70 cm to 60 cm patient bore. Thus, this parameter is a crucial part of the MR system concept definition. It emphasizes the importance of efficient use of radial space inside the magnet bore. The best gradient performance is achieved by using only the necessary number of windings driven by the highest available current. In practice, the maximum current is mainly limited by power amplifier technology, forces on gradient connectors, wire cross section, and cooling efficiency. Additional design targets like shielding efficiency, force/torque compensation, and acceptable nonlinearities of the linear gradient field tend to increase the required number of windings, making up the challenge to the coil designer (Fig. 4).

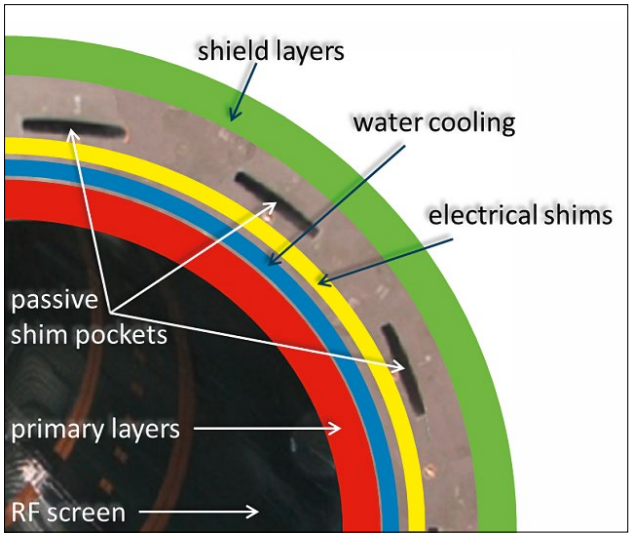

5 Layer breakdown of a cylindrical gradient coil system including passive iron shim.

Cylindrical symmetry dominates today's gradient coils. Coil geometry mostly follows the boundary conditions set by the main magnet design. Insert gradients could be designed without following the basic symmetry of the main magnet, but hardly do so. Due to the non-ideal nature of magnet and gradient fields (e.g. concomitant fields, forces, and torques), it is always advantageous to keep as many symmetries as possible. Dedicated insert gradients for different body parts are known (for example spine or knee [18]), but have not been successful in replacing their big brothers. Electrical and mechanical design aspects of non-cylindrical geometries are not very different from the standard configurations. For example, the target field method could be applied to calculate the primary and the shields' current density on a circular plane. The wire pattern and axial connections are generated by extracting the contour lines of their stream function. The same method can be applied to generate the wire pattern for

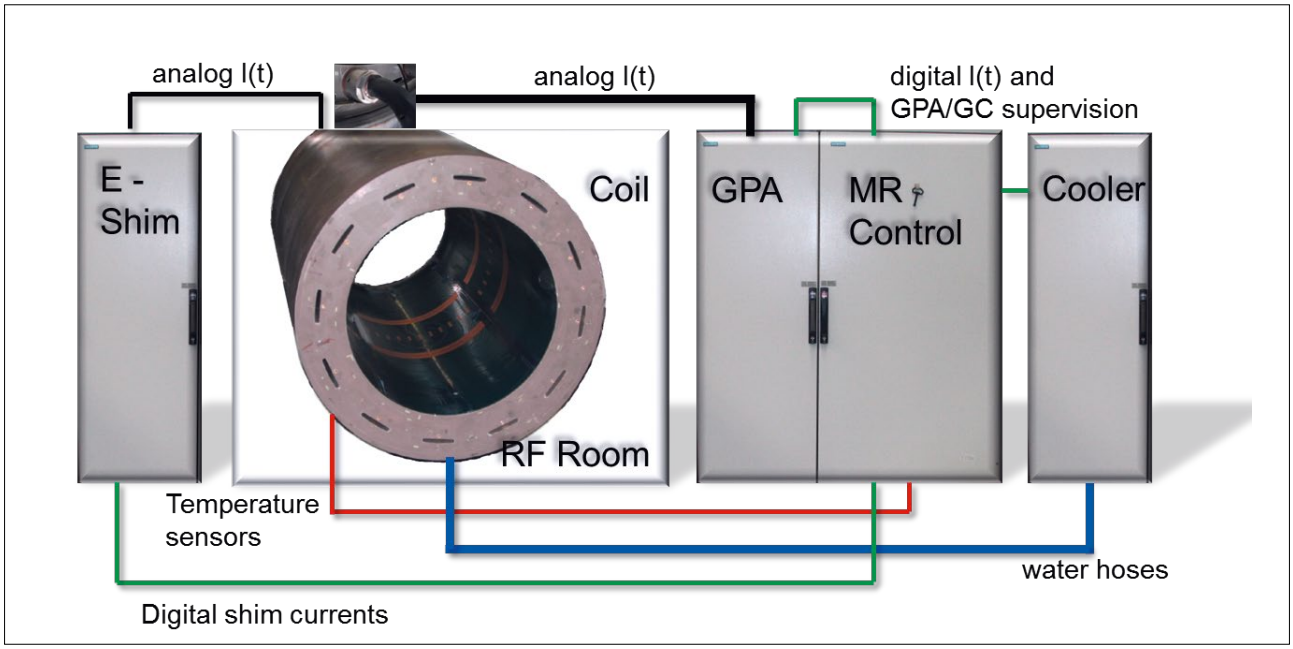

6 The gradient system consists of a coil system, a cooling system, a gradient power amplifier (GPA), a shim amplifier, and a gradient control system as part of the MR control system.

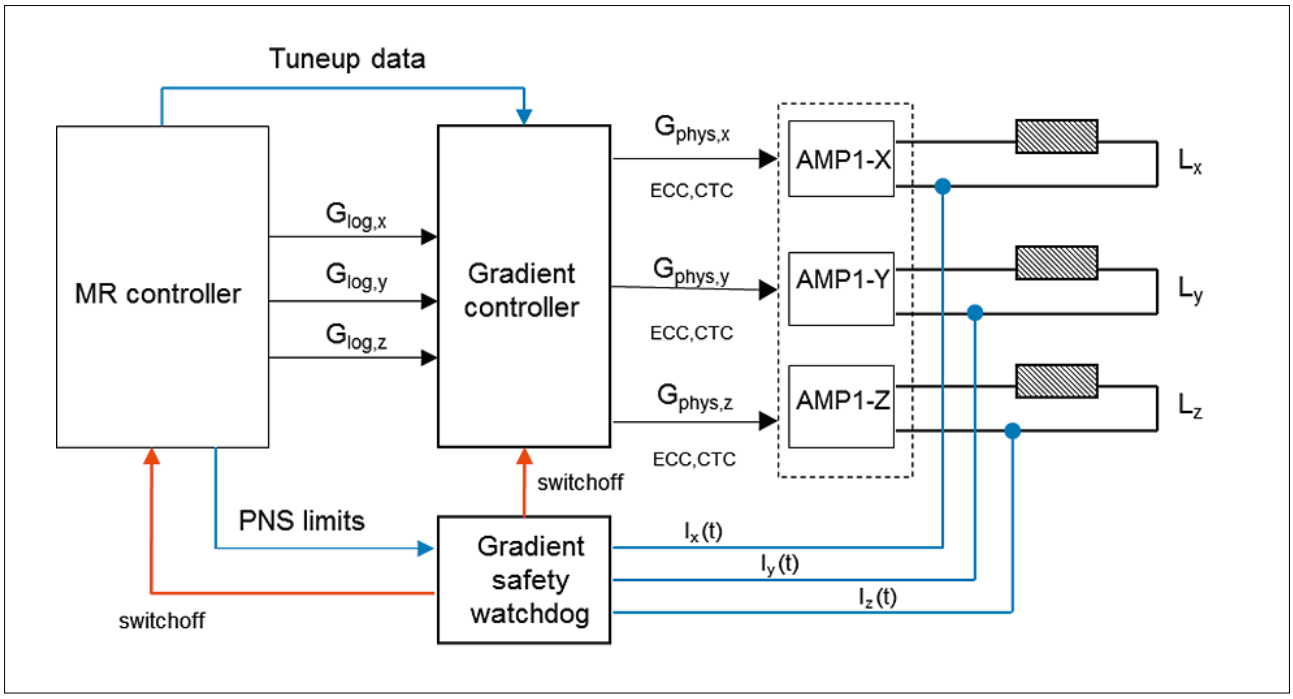

7 Control system of a typical MR scanner and its interface to the gradient controller. The gradient controller and the PNS safety watchdog are fed with logical gradient shapes (G_{log}) and gradient-coil-specific limits for peripheral nerve stimulation. The logical shapes are converted to physical shapes (G_{phys}) and modified by filter functions for eddy current and cross-term compensation (ECC and CTC) before being fed to the gradient amplifier's final stages (Amp X, Y, Z). The current in the gradient circuit with the coil impedance L is measured by high precision current probes and fed to the gradient safety watchdog unit. In case the PNS limit is exceeded, a safety switch-off signal is sent to the gradient and MR controller.

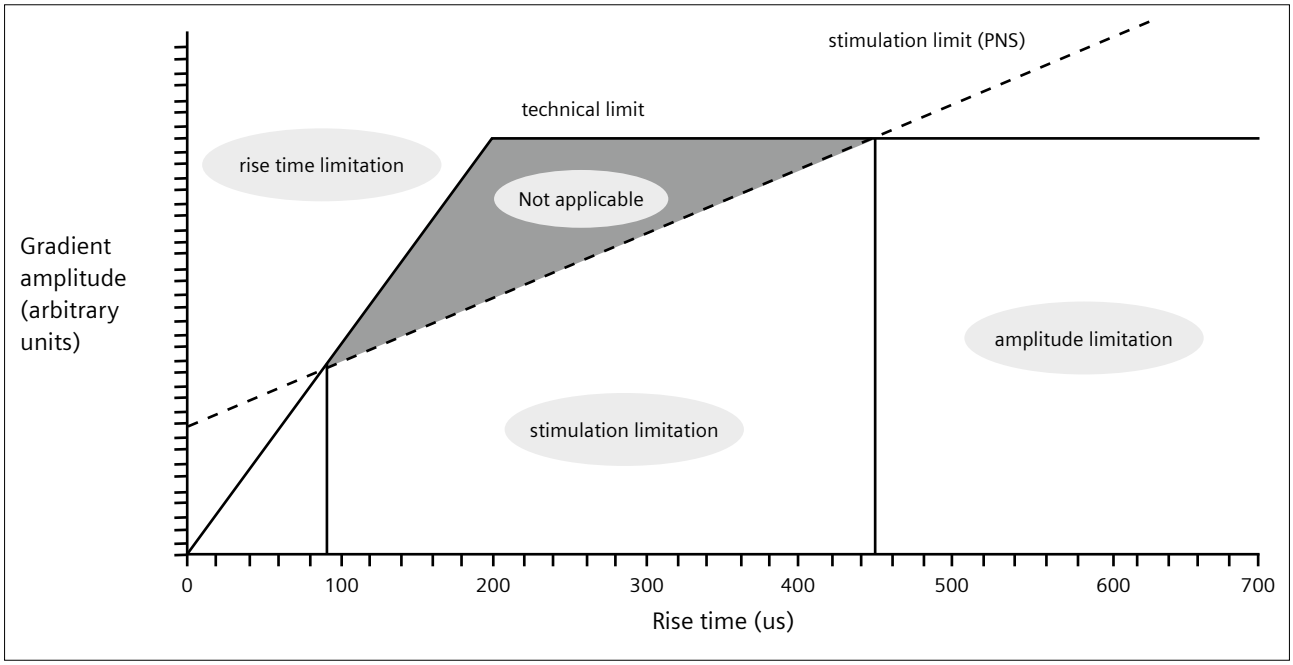

8 Limitations of gradient system performance for human use. The main limitation is given by the peripheral nerve stimulation threshold (PNS limit). If the technical performance of the gradient system is not adapted to this limit, a significant part of the parameter space is not applicable to human subjects.

the electrical shim coils. The gradient system thus consists of a variety of complex subcomponents, each forming a subsystem of its own (Fig. 6). The coil system (Fig. 5) comprises the linear field coils (X, Y, Z) including their shielding coils, higher-order shim coils, cooling layers, temperature sensors, RF screen, current and water connectors, the coil support structure, and its suspension.

Magnetic field generation with high amplitudes and large volumes is a difficult task. Considering that the natural (earth) magnetic field is about 50 uT in amplitude, the first whole-body gradient coils had to exceed this by two orders of magnitude. In one embodiment, wooden structures were used to support the race-track-like windings (Fig. 2). Furthermore, rapid gradient switching leads to strong vibrations due to the Lorentz forces of the conductors within the main magnetic field. This can be counteracted by increased stiffness of the support structures (e.g. with glass-fiber-reinforced plastic) and linking of all layers to a single body (e.g. with epoxy resin). In addition, dielectric strength of all gradient layers is required at minimal (<2 mm) radial distance of the conductors. Hence, today's gradient coils mainly consist of epoxy resin with excellent dielectric strength at low cost and high geometric flexibility. The challenge in the fabrication process is to ensure that all layers and subcomponents of the coil system are impregnated 100%. This can only be achieved with a complex vacuum potting procedure. Every step of this procedure needs to be defined and controlled thoroughly [19]. Process and material parameters like temperature profile, filling material, and filling percentage as well as curing time need to be adjusted to the geometry and inner structure of the gradient coil main body. A successful potting procedure is usually validated with a high voltage or electrical discharge test. This step ensures that the dielectric strength is good enough to withstand amplifier voltages of up to several kilovolts for an MR system's lifetime.

The control system of an MR scanner synchronizes and drives the activities of all hardware components (Fig. 7). The interface of the MR controller to a logical hardware component usually requires a sub control system of its own. The gradient controller and the Peripheral Nerve Stimulation (PNS [20]) safety watchdog are fed with logical gradient shapes (read, phase, slice) and gradient-coil-specific limits for PNS, respectively. Static correction data acquired during the first startup phase of the MR scanner ('Tune-up data') is transferred to the gradient controller and GPA before the start of the measurement sequence.

After the start of a gradient pulse sequence, the logical gradient shapes are converted into physical gradient shapes. In order to minimize eddy current effects, additional filters based on tune-up data may be applied to the gradient circuit current I(t) before transfer to the gradient amplifier component (e.g. eddy current pre-emphasis). The output of the gradient amplifier circuit is monitored by high-precision current sensors. Their signal is used for control and supervision of the gradient amplifier cabinet including PNS. The limits for human exposure to time-varying magnetic fields are defined by the IEC norm and need to be ensured based on calculations and measurements (Fig. 8).

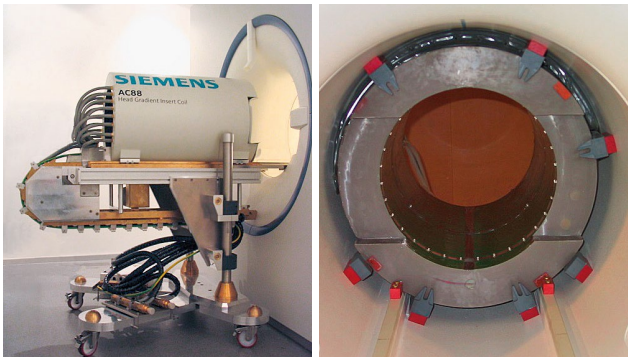

7 Gradient insert 'AC88'. **(9A)** Test of the handling device at a 3T scanner. **(9B)** Reduced size of patient bore after installation of the coil.

Ultra-high gradient strength

The first decade of the new millennium brought the benefits of parallel imaging methods from research machines to clinical MRI scanners. Today (2017), most sequences make use of acquisition methods with measurement time reduction (or, in case of EPI, readout time reduction). Although the demand for high gradient amplitudes for diffusion imaging techniques is still unbowed, the advantage of ultra-high gradient slew rates now has a serious competitor.

Implementation of ultra-high gradient amplitudes with head-sized gradients inside a whole-body magnet bore is one approach to tackle the problem [21]. The advantage of simultaneous ultra-high slew rate and gradient amplitude is counteracted by the limited space inside the coil (Fig. 9). It is difficult to design a combined transmit/receive RF coil with >8 receive channels, good intra-channel decoupling, and high SNR due to the close proximity to the copper windings of the gradient coil. Separating the transmit coil is even more challenging, as this requires additional radial space for the RF return flux. In addition, patient handling is difficult. It is not easy to find volunteers who are willing to expose them-selves to the near-claustrophobic conditions of such an experimental device. Even with asymmetric gradient design, the limited size of the shoulder cutouts will exclude part of the normal population from being scanned.

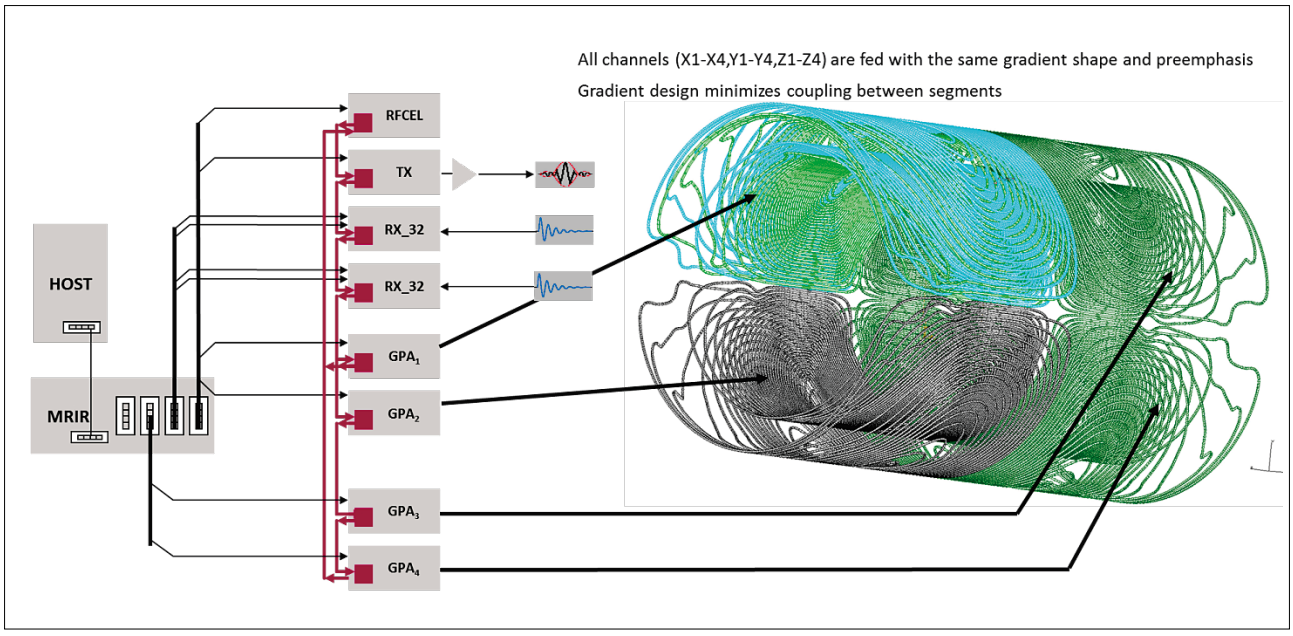

10 Control system concept for the 300 mT/m gradient. The MR control system (host computer HOST, image reconstruction computer MRIR) was extended to drive four sets of gradient amplifiers independently. The new architecture allows storing the calibration data for each of the 12 final stages driving the gradient coil segments.

In diffusion imaging of the brain, long-lasting diffusion weighting gradient lobes are applied. The highest possible gradient amplitude is applied in the shortest possible time, combined with an echo-planar imaging (EPI) pulse sequence to encode diffusion and minimize head motion at the shortest possible echo time (TE). Typical TEs for b = 1,000 s/mm2 on a 3T whole-body scanner are around 70–80 ms when Stejskal-Tanner encoding is applied without additional parallel imaging techniques. Higher b-values can only be achieved with a penalty in SNR, as TE increases with the duration of the diffusion lobe. Studies on mammals have indicated that much higher gradient strength than 40 mT/m would be required to produce sharp diffusion images of an adult human brain's wiring patterns [22]. Typical small-bore (about 100 mm) NMR scanners can apply 150–300 mT/m. Owing to the nonlinear increase of gradient strength with reduction of the inner diameter, even 1,000 mT/m (at 60 mm bore) are not uncommon. This reopened the question whether ultra-high gradient strength (>100 mT/m) may be achievable with a whole-body gradient design. The design target for a whole-body gradient was set to high gradient amplitudes with the linearity volume (LV) being limited to the brain volume (thus achieving less restrictive PNS thresholds). Two versions of this gradient design were designed and built. Version 1 (SC72) supports a G_{max} of 100 mT/m at SR 200 T/m/s with a single GPA cabinet (2 kV, 1 kA). It was designed to match forces and stray field of a 3T magnet and provide space for passive iron shims. It has a length of 158 cm, and an inner diameter of 64 cm. This yielded a robust, easy-to-use diffusion engine [23].

Version 2 (AS302) represents a quantum leap in whole-body gradient performance, i.e. G_{max} of 300 mT/m at SR 200 T/m/s. Design studies with reduced linearity constraints showed that up to 150 mT/m could be reached with a single gradient power amplifier. A further increase of gradient strength within conventional design constraints would have imposed duty cycle limitations, which are not favorable for diffusion applications. Due to the large volume of the coil body, the number of current density layers and thus the gradient strength could be doubled to 300 mT/m. As a consequence of the mutual coupling of the four primary and secondary layers per axis, coil inductance increased by more than a factor of two. To drive this high inductance at the SR 200 T/m/s needed for EPI readout, a new gradient system concept involving multiple gradient amplifiers was developed. In order to achieve the target slew rate, each of the three axes X, Y, Z was split into four independently driven segments (Fig. 10). Stray field and forces were matched to the 3T magnet used. The MR control system was extended to drive four sets of gradient amplifiers independently. The new architecture allows storing the calibration data for each of the 12 final stages driving the gradient coil segments. The gradient waveform

11 Modified MAGNETOM Skyra system. Dimensions of the RF body coil, patient table and cover were adjusted to the size requirements of both Connectom gradient coils.

is logically split and fed to four individual gradient controllers. This architecture also allows generating arbitrary field characteristics for each gradient coil axis, used to optimize eddy current compensation.

The GPA regulator architecture was extended to account for the dynamic differential control (D) of the driving signal. This allows counteracting the induced voltages in each segment coil due to mutual coupling. A new RF body coil was developed (capable of TrueForm excitation) which allows the use of the existing clinical patient table with minor mechanical modifications. The covers were modified accordingly (Fig. 11). Three cooling cabinets, four GPAs and a second filter panel were installed in the equipment room, before the first phantom images could be acquired in May 2011. Measurements of acoustic noise and vibrations showed lower amplitudes than typical 3T scanners, which is in line with the larger mass of the gradient coil body and the related higher net precision of torque and force balancing methods. The PNS studies performed on the AS302 and SC72 coils confirmed that it is possible to use high EPI readout amplitudes without PNS effects. Long rise times at high-amplitude pulses are limited by the regulatory-required cardiac monitor which was implemented in hardware.

Research in the US

Achieving the current state of connectomics has required a huge increase in MRI sensitivity, as well as much higher processing speeds to cope with the large amount of spatial data from water molecules. Unlike the BOLD effect which experiences enhanced contrast as field strength is increased, the diffusion contrast is set only by the displacement of the water and the applied field gradient and is thus independent of B_0. On the other hand, a more than two-fold sensitivity increase at 7T field strength would offer the opportunity to increase resolution for whole-brain studies towards one-millimeter isotropic voxel size. As the available methodologies in 2011 were not up to routinely coping with shorter T2 and T2* relaxation times, increased $B_1(+)$ inhomogeneity and increased power deposition (SAR) at >7T field strength, both WU-Minn and MGH-UCLA teams set their main focus on 3T.

The MGH-UCLA consortium decided to re-engineer their scanner from the ground up to optimize diffusion imaging. Their efforts went into ultra-high gradient strength, sequence design and reconstruction, and high-channel receive coils. The gradient system with 300 mT/m was a major focus since gradient amplitude is central for the parameters diffusion contrast, T2 signal loss, and probability density function (PDF) of water. A field-of-view (FOV) shifting approach to Simultaneous Multi-Slice (SMS) EPI [25–27] was chosen to enable whole-brain coverage with low TR and TE. The group developed a 64-channel brain array coil showing a relative SNR gain of at least 40% compared to a sized-matched 32-channel brain array within the peripheral brain ROI [28]. The achieved efficiency gain is more than a factor of eight for high-b-value diffusion (3.5 x from shorter TE, 1.7 x from the slice acceleration factor of 3 from SMS, and 1.4 x from the RF coil) [29]. Average scan time for whole-brain diffusion was shown to be reduced from about one hour to 15 minutes (combined with compressed sensing, scan time was <5 minutes).

Increasing the gradient strength to the highest value ever attempted for human imaging also has significant impact on the concomitant field terms. In comparison to a conventional 45 mT/m scanner at 3T, the maximum field pertubation increases by a factor of $\sim(300/45)^2 = 44$. The MGH-UCLA group successfully tackled this problem with the implementation of a fully refocusing Stejskal-Tanner scheme [1] and accompanying pre-processing eddy current correction. An unanticipated finding was that the increased gradient strength could induce magneto-phosphenes in the subjects' eye retina. Lowering the head coil vertically and positioning the eyes at isocenter in z was found to eliminate the induction of magneto-phosphenes within volunteer studies.

The ultra-high gradients yielded substantial and immediate gains in the sensitivity through reduction of TE while improved signal detection (Fig. 12) and increased efficiency of the DSI or HARDI acquisition, accuracy and resolution of diffusion tractography were illustrated (Fig. 13). Comparisons were performed across b-values based on q-ball orientation distribution function (ODF) metrics to investigate whether high-b-value diffsusion imaging (dMRI) (up to 10 k s/mm^2) can improve resolving

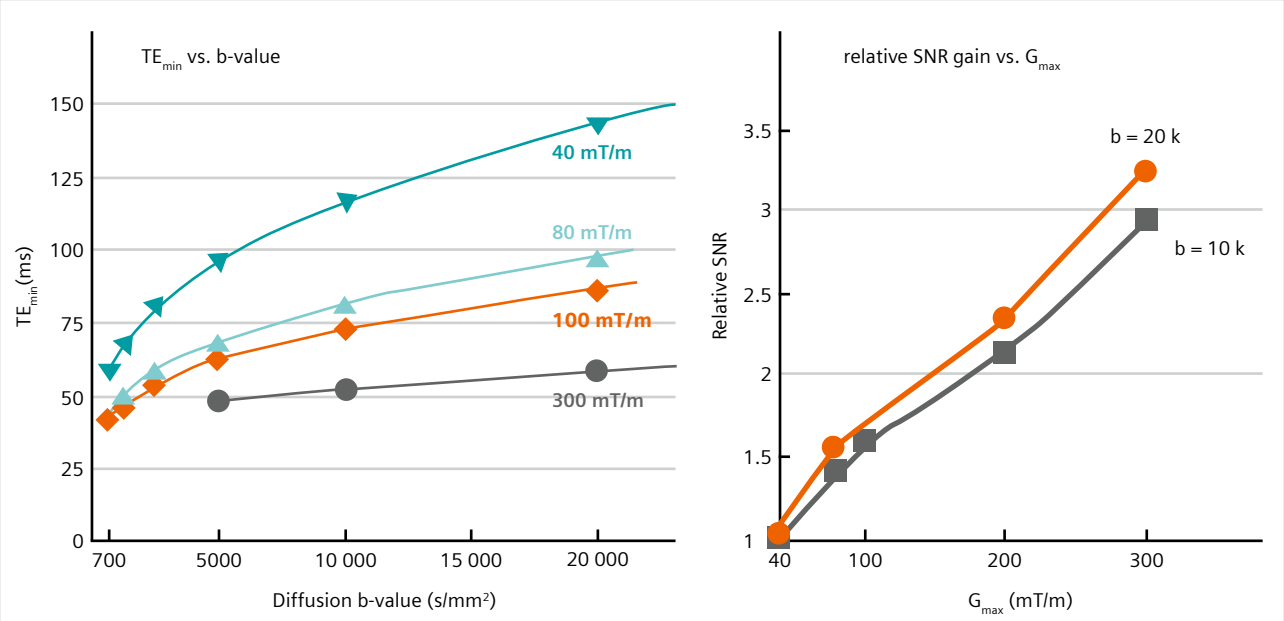

12 **(12A)** Minimum TE for a Skeskjal Tanner diffusion sequence (2 mm isotropic, FOV 200 mm). **(12B)** Measured SNR of the brightest sections of *in vivo* human white matter with 64-channel brain array coil (b = 10,000 s/mm² and 20,000 s/mm²).

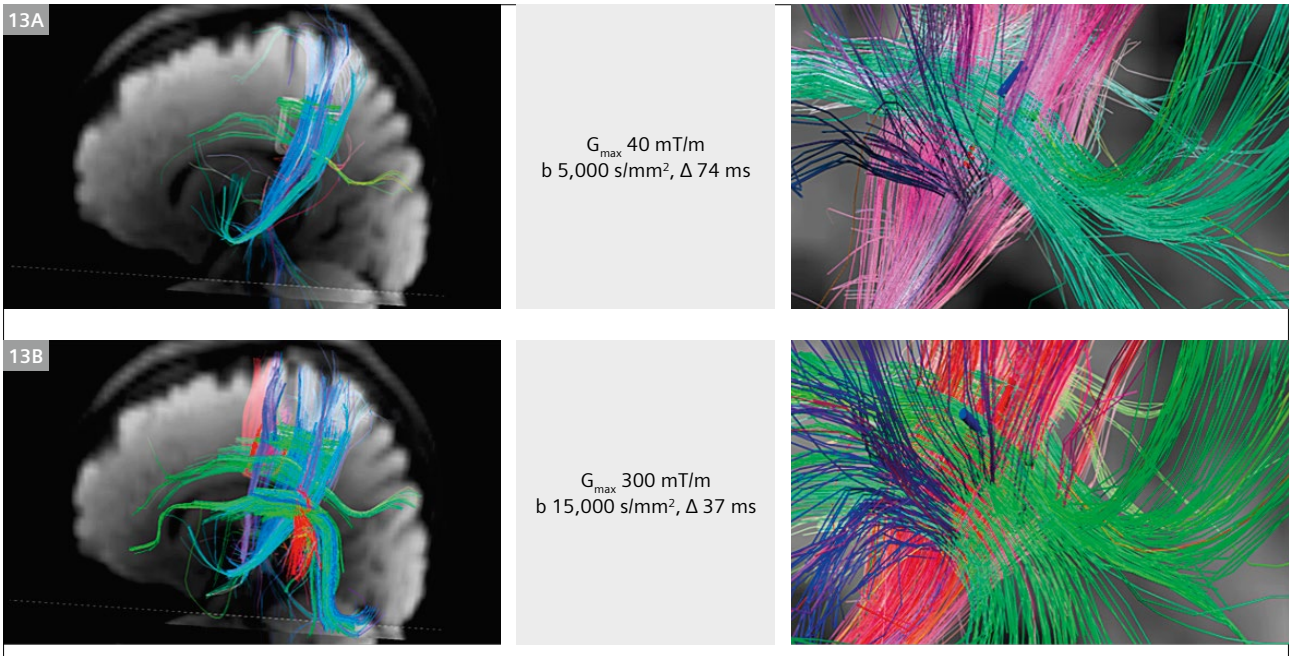

13 Micro-structural resolution with 40 mT/m **(13A)** and 300 mT/m **(13B)** gradients. dMRI data was aquired with a b-value of 5,000 s/mm² and 15,000 s/mm² respectively. Fiber pathways were computed with deterministic streamline integration and show a higher level of detail with a b-value of 15,000 s/mm². *Images courtesy of MGH, Boston, USA.*

complex white-matter structures. The q-ball ODF features became sharper as the b-value increased. Crossing structures were detected in an encreasingly larger fraction of white-matter voxels, and the spatial distribution of two-way and three-way crossing structures was found largely consistent with known anatomy (Fig. 14). Results indicate that dMRI with high diffusion encoding is a promising tool to characterize and understand the underlying structural organization and topological paths (motifs) in the human brain [30].

Relationships of adjacency and crossing between cerebral fiber pathways in humans and in nonhuman primate species are a major focus of the Connectomics department at the MGH. Whole-brain diffusion spectrum MRI was acquired with the 300 mT/m scanner *in vivo* in subjects (515 directions; pathways were computed with deterministic streamline integration, see Figs. 15–17) and *ex vivo*.

The cerebral fiber pathways were seen to form a rectilinear three-dimensional grid continuous with the three principal axes of early development. Cortico-cortical pathways were observed to form parallel sheets of interwoven paths in the longitudinal and medio-lateral axes, in which major pathways were local condensations. Details are covered by a *Science* publication from 2012 [31].

Beyond the immediate scope of the HCP, further applications like brain recovery after traumatic coma, axon diameter distributions [32, 33], and post-mortem diffusion tractography were explored. It could be shown that ultra-strong gradients enable human applications of techniques that were previously possible only in small-bore scanners. Detailed research results were published by Neuroimage [34] in 2013. More than 60 subjects were scanned with the 300 mT/m system by the MGH-UCLA consortium. The resulting reference data base was made publically available on the HCP internet homepage in 2016 [35].

The WU-Minn consortium focused on mapping long-distance brain connections [36] and their variability within healthy adults (twins and their non-twin siblings [37]). Three complementary methods were used, namely resting state functional MRI (rfMRI) which uses correlations in the temporal fluctuations in an fMRI time series to derive 'functional connectivity'; dMRI, which provides the input for axonal fiber tractography; and task-based fMRI (tfMRI), which is used together with T1- and T2-weighted imaging to identify functional parcellation in the human brain [38]. Improvements and optimization of these methods (Multiband/Simultaneous Multi-Slice Imaging) resulted in a whole-brain coverage with 2 mm isotropic resolution

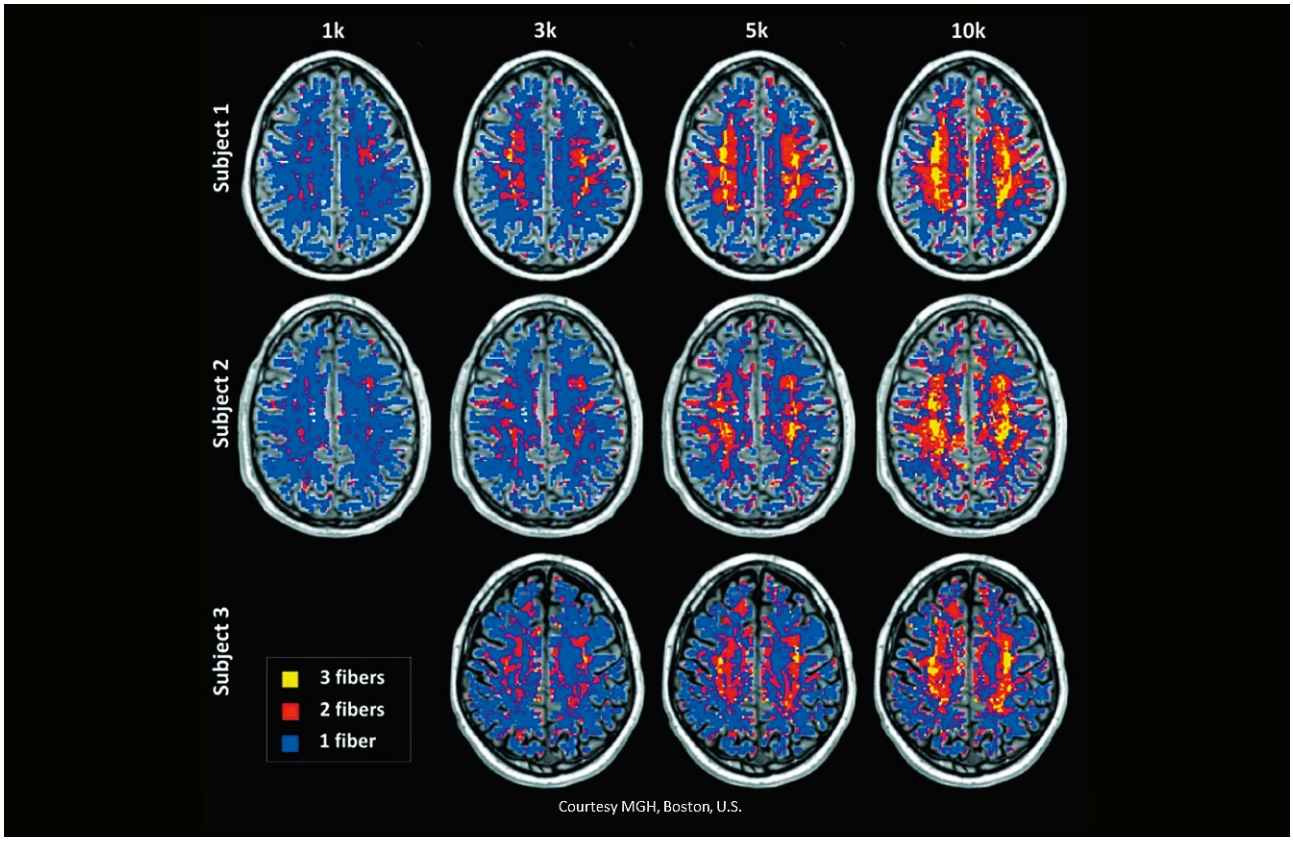

14 Spatial distribution of the number of fibers per voxel within the brain of three subjects (blue = 1, red = 2, yellow = 3 or more fibers). The orientation distribution function (ODF) peak threshold was selected to be two times the standard deviation above the mean of the noise peaks. A higher percentage of white matter voxels was identified as containing crossing fibers as b-value increased from 1,000 to 10,000 s/mm^2.

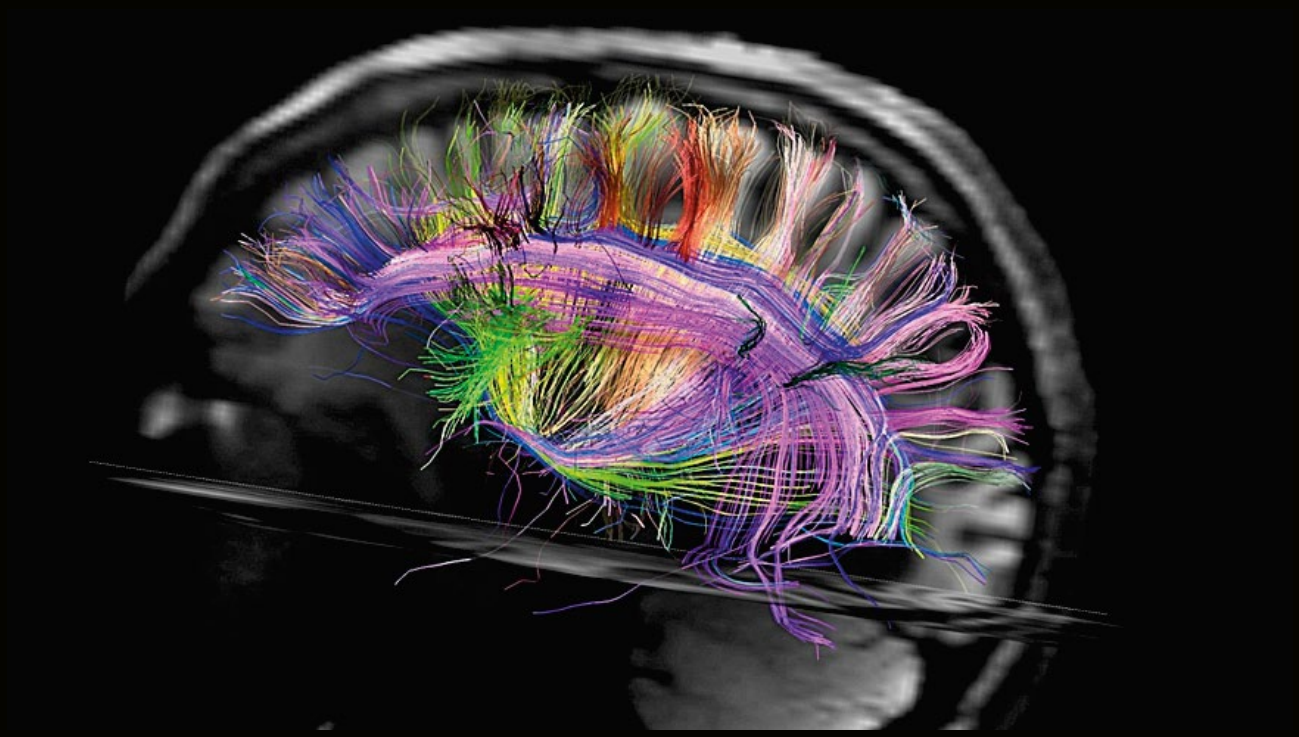

15 *In vivo* diffusion spectrum imaging (DSI) of the human brain. Reconstructed nerve fibers show the grid of corona radiata and SLF. Resolution 1.5 mm^3, max b-value 15,000 s/mm^2, TA 20 min. *Image courtesy of V. Wedeen, MGH, Boston, USA.*

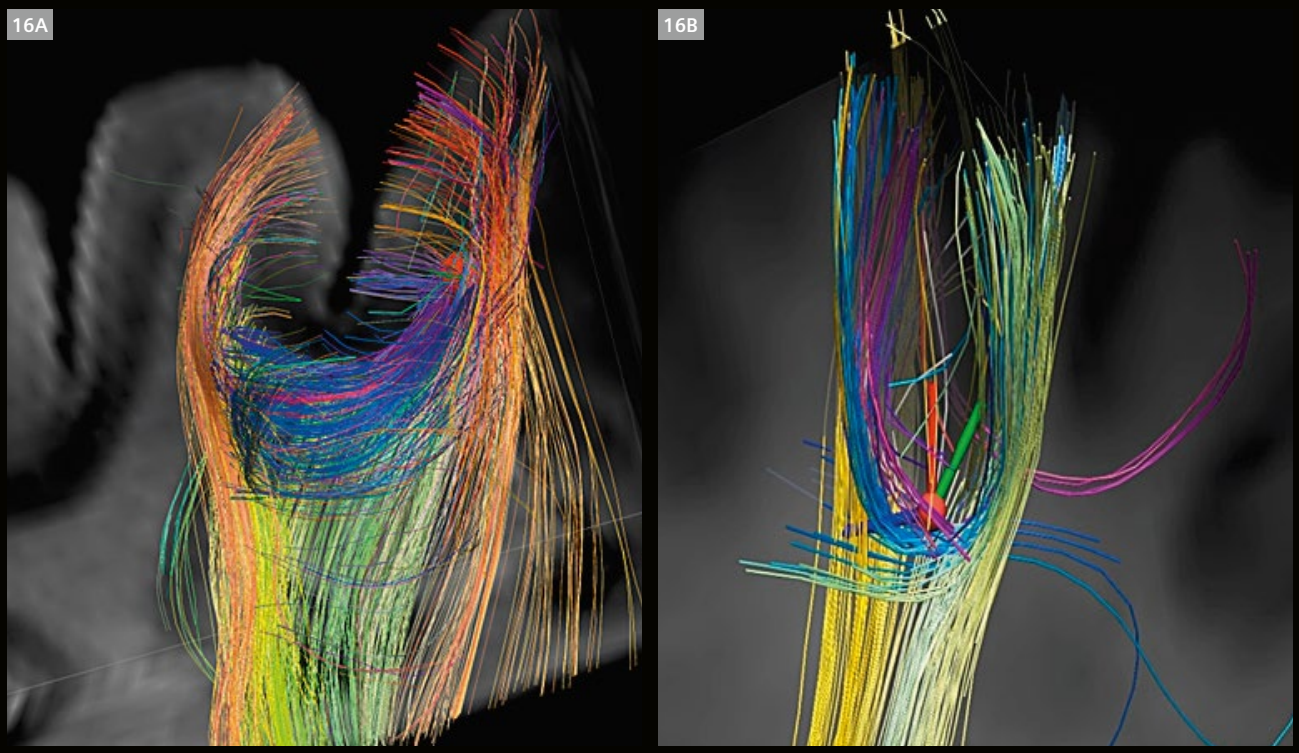

16 Diffusion spectrum imaging (DSI) of the human central sulcus U-fibers. **(16A)** *Ex vivo* data (b-value 40,000 s/mm^2, voxel size 0.5 mm^3 isotropic, TA 12 h). **(16B)** *In vivo* data (b-value 15,000 s/mm^2, voxel size 2 mm^3 isotropic, TA 20 min). *Images courtesy of V. Wedeen, MGH, Boston, USA.*

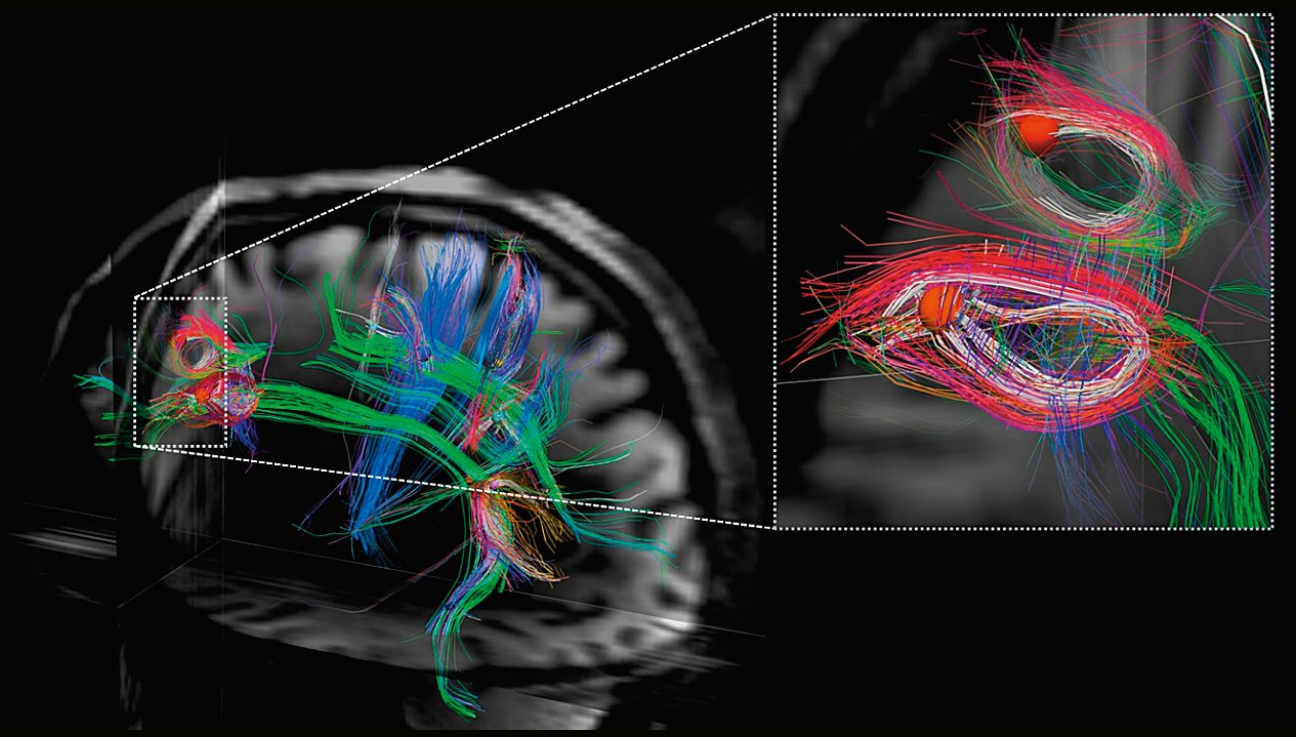

17 *In vivo* diffusion spectrum imaging (DSI) of the human gyri, and its continuity with deep white matter. (b-value 15,000 s/mm², voxel size 1.5 mm³ isotropic, TA 20 min). *Image courtesy of V. Wedeen, MGH, Boston, USA.*

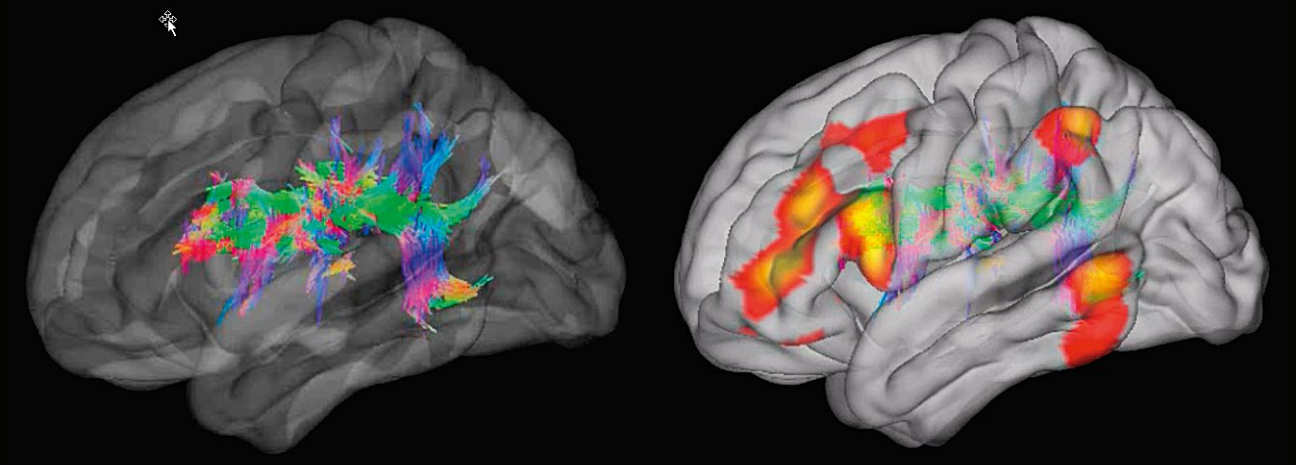

18 Interactive composite dataset of the human brain (180 areas per hemisphere). Red and yellow sections are based on data from resting state functional MRI, whereas the multicolored fibers were generated using probabilistic streamline tractography based on diffusion MRI. *Images courtesy of Washington University – University of Minnesota – Oxford University Human Connectome Project.*

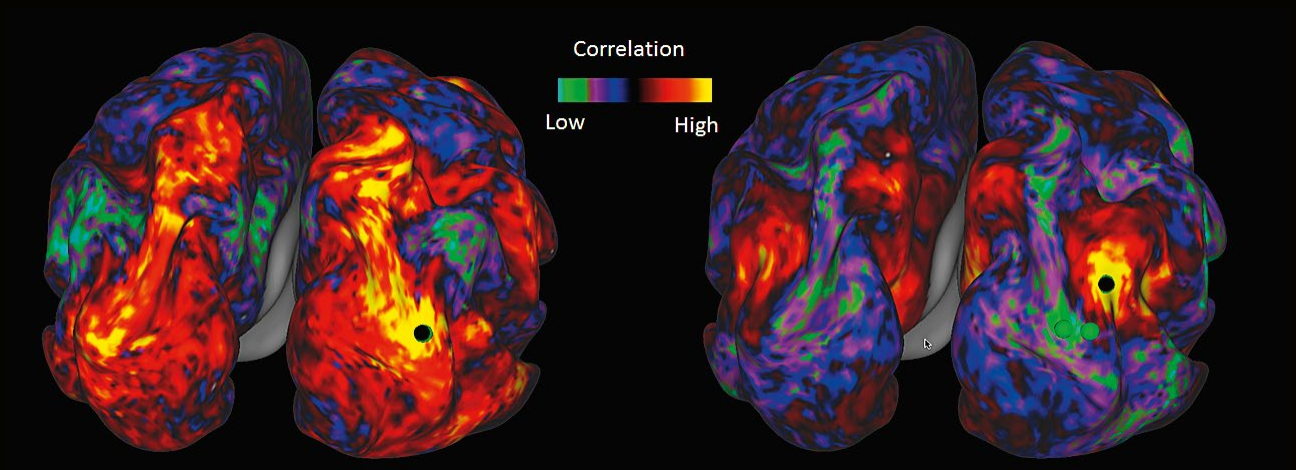

Group average, HCP Pilot-1 dataset (10 subjects, 14 scans), MB = 4, TR = 1.4 s, 2 mm voxels

19 Interactive composite dataset of the left and right cerebral hemispheres of the human brain (group average of 10 subjects). Red and yellow sections are strongly related to the seed location (black dot). The correlation factor is based on data from resting state functional MRI.
Images courtesy of Washington University – University of Minnesota – Oxford University Human Connectome Project.

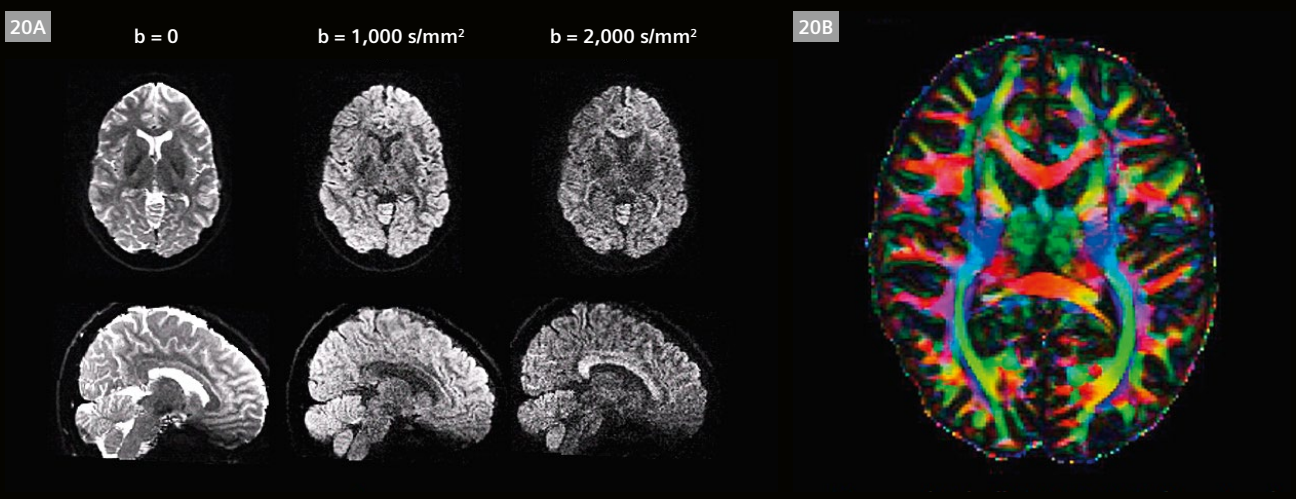

MB3, 100 mT/m, 1.25 mm isotropic

FA map (3 shell HARDI, 270 directions)

20 Representative examples of diffusion MRI with the finalized 3T HCP protocol (100 mT/m, MB3, 1.25 mm^3 isotropic). Anatomical detail in comparison to a conventional 3T protocol (2 mm^3 isotropic, not shown here) is significantly improved. **(20A)** Image intensities are presented in arbitrary units after distortion correction and averaging across paired phase encoding directions. **(20B)** Color fractional anisotropy (FA) maps. Colors depict the principal fiber orientation and gray scale intensities are defined by FA.
Images courtesy of Washington University – University of Minnesota – Oxford University Human Connectome Project.

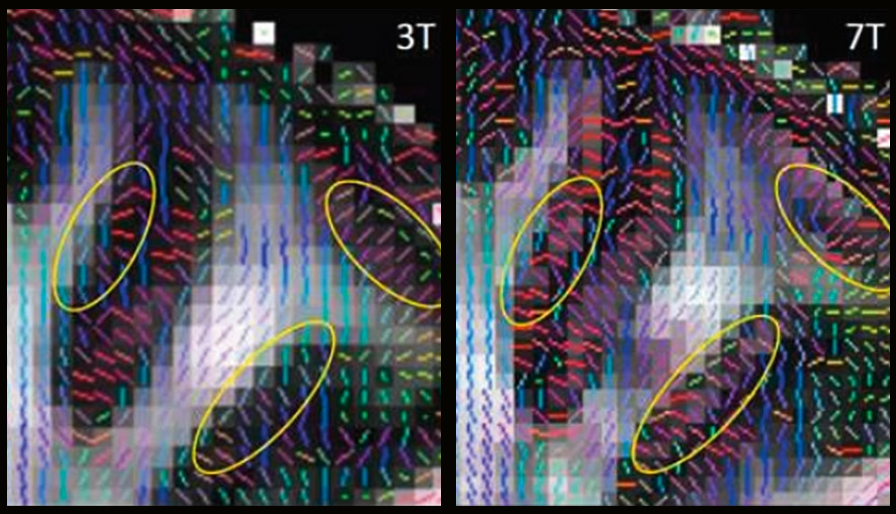

MB3, 100 mT/m, 1.25 mm isotropic

iPAT3, MB2, 70 mT/m, 1.05 mm isotropic

21 Zoomed-in coronal view of DTI principal direction of diffusion (PDD) maps overlaid on corresponding fractional anisotropy (FA) maps. HCP 3T **(21A)**. 7T **(21B)**. Due to the higher resolution and reduced partial volume effects, the 7T data recovers gray matter regions of low FA (yellow circles). *Images courtesy of Washington University – University of Minnesota – Oxford University Human Connectome Project.*

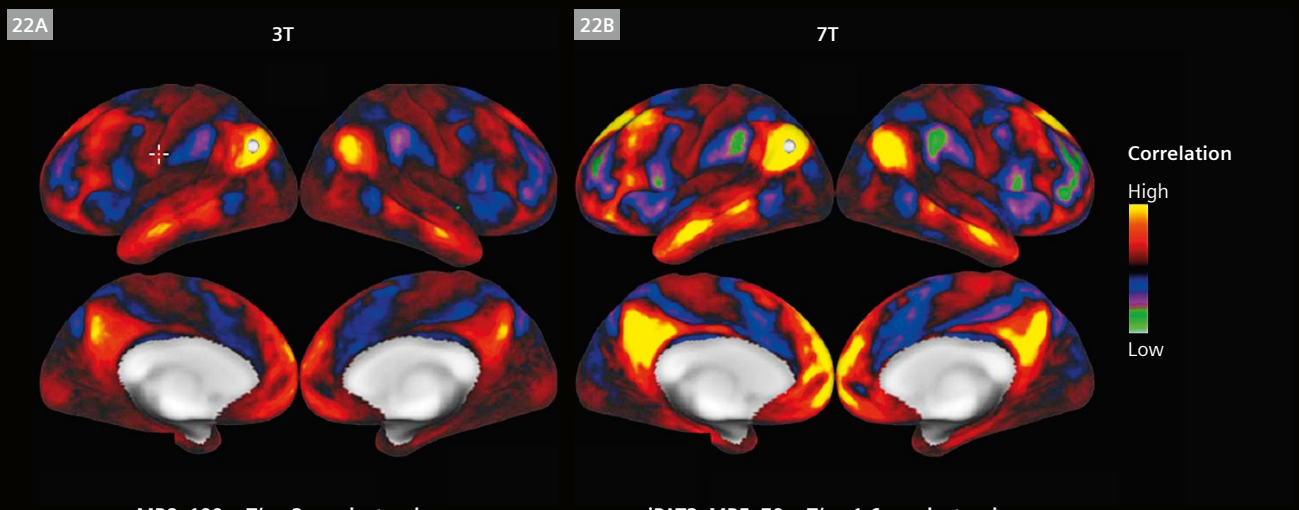

MB8, 100 mT/m, 2 mm isotropic

iPAT2, MB5, 70 mT/m, 1.6 mm isotropic

22 Exemplary composite dataset of the left and right cerebral hemispheres of the human brain (3T vs. 7T). Red and yellow sections are strongly related to the seed location in occipital parietal cortex (white dot). The correlation factor is based on data from resting state functional MRI. While the 3T data shows detailed connectivity / correlation throughout the brain, the correlation factor of 7T data is even more pronounced. *Images courtesy of Washington University – University of Minnesota – Oxford University Human Connectome Project.*

in 0.7 seconds for fMRI, yielding a data acquisition speed-up factor of up to nine. Applied to 1.25 mm isotropic dMRI data, a three-fold reduction in total data acquisition time was achieved. Using the HARDI [10] approach, diffusion encoding was performed with 270 q-points distributed over three shells of b = 1,000, 2,000, and 3,000 s/mm^2 (Fig. 20). Due to the targeted high number of subjects, the robust and easy-to-handle 100 mT/m gradient system was chosen.

The first half of the 5-year project focused on refining methods for data acquisition and processing [39] and resulted in robust fast pulse sequences and pre-processing pipelines providing substantial improvements for each of the MRI modalities [40]. The first pipeline provides correction algorithms for MRI raw data (e.g. eddy current and spatial distortion correction, reduction of temporal artifacts. The second pipeline involves mapping the data to cortical surfaces and subcortical gray-matter domains (Fig. 18), as understanding the human cerebral cortex requires a map (or parcellation) of its major subdivisions. Based on a pilot study of 10 healthy adults, an interactive composite dataset of the left and right cerebral hemispheres was created (Fig. 19). Red and yellow sections are strongly related to the seed location (black dot). The correlation factor is based on data from resting state functional MRI. This methodology could take research to a different level, considering that mental illnesses like autism might be related to abnormal brain circuits showing up a reduced functional connectivity in rsMRI scans.

Using multi-modal MRI images, 180 areas per hemisphere were delineated, bound by changes in cortical architecture, function, connectivity, and/or topography in a group average of 210 healthy adults. It has been possible to characterize 97 new areas and 83 previously reported areas. Automated delineation and identification of these areas was supported by a machine-learning classifier. This classifier detected the presence of >95% of the cortical areas in new subjects, replicated the group parcellation, and could correctly locate areas in individuals with atypical parcellations. These tools and datasets are part of the *'Connectome Workbench'* and *'ConnectomeDB'* database and were made available to the public [41].

After finalizing the HCP protocols in 2012, data was acquired using multiple imaging modalities, including customized 3T MRI (1,200 subjects) and 7T MRI (200 subjects) plus combined magneto- and electro-encephalography (MEG-248-channel/EEG-64-channel, 100 subjects). Technical optimizations in 7T image acquisitions for the HCP allowed to obtain high-quality, high-resolution whole-brain *in vivo* dMRI data (Fig. 20). These data show spatial details typically seen in ex-vivo studies and complement already very high-quality 3T HCP data in the same subjects [42]. More recently [43], it could be demonstrated that high-resolution images acquired at 7T provide increased functional contrast-to-noise ratios with significantly less partial-volume effects and more distinct spatial features (Figs. 21, 22). Studies of structural and functional brain connectivity were paired with behavioral and heritability measures. A detailed summary of the 5-year project result was published in *Nature Neuroscience* [44].

Research in Europe

The scientific success of the Connectome gradients has recently persuaded two major European research centers to extend their instruments parks with a 300 mT/m machine. **The Max Planck Institute for Human Cognitive and Brain Sciences, Leipzig, Germany**, plans to develop MRI methods to reliably characterize the detailed functional and anatomical micro- structure of the human brain. Their strategy is to combine the best data from 7T and the 3T Connectom scanner. They plan for imaging the intracortical microstructure, such as myeloarchitecture and intracortical connectomics, and fine structure in the white matter. The ultimate goal is to understand the structure-function relationship in the human brain, pathological changes in neurodegeneration (e.g. amyloid plaques in Alzheimer's disease) and provide early biomarkers. A first step in methodology development will comprise high-fidelity field mapping, optical prospective motion correction and new pulse sequences, in order to achieve a spatial resolution of 600 um or higher combined with high diffusion-weighting factors.

The **Cardiff University Brain Research Imaging Centre (CUBRIC), Cardiff, UK** plans to develop MRI methods for quantifying tissue structure at the microscopic scale. The principal approach looks at how fine tissue structure impedes the movement of water. Current MRI hardware (i.e. gradient strength) restricts measurement to relatively large molecular displacements and from tissue components with a relatively strong and long-lived signal, prohibiting quantification of individual cell dimensions, or packing of nerve fibers. Once achieved with the new 300 mT/m machine, faster acquisition and access to newly-visible signal components will enable new mathematical models of microstructure on finer length-scales. This will help to increase understanding of tissue structure in health and disease, and to make testable predictions on important biophysical parameters such as nerve conduction velocities in the brain or cell structure in the liver. The ultimate goal is to develop the imaging software that brings this hardware to mass availability, in turn enabling a new generation of mainstream microstructure imaging and macrostructural connectivity mapping techniques to translate to frontline practice.

Conclusion

As of today, more than 140 studies have acknowledged the use of data generated by the Human Connectome Project. This reflects the goal of the NIH funding organization, which intended that the findings should be broadly applicable to clinical and scientific questions. Both MGH-UCLA and WU-Minn consortia, have successfully developed and applied new methods to map structural and functional connectivity of the brain. Gains in spatial sharpness and clarity are qualitatively analogous to those made in astronomy after the introduction of adaptive optics to overcome the atmospheric blurring. The initial thought that the human brain could be mapped in analogy to the Human Genome Project is now supported by a first, but important step. A promising next step is the extension of the Connectome user base with the new European sites, Cardiff University Brain Research Imaging Centre (CUBRIC) and Max Planck Institute for Human Cognitive and Brain Sciences, Leipzig. It remains to be seen in the future, which further methodical and instrumental steps need to be taken until the level of understanding of the human brain approaches that of *C. elegans*.

References

1 Stejskal EO, Tanner JE. Spin diffusion measurements: spin echoes in the presence of a time-dependent field gradient. Journal of Chemical Physics. 1965;42:288–292.s

2 Le Bihan D, Breton E (1985). Imagerie de diffusion in-vivo par résonance magnétique nucléaire. C R Acad Sci (Paris). 301 (15): 1109–1112.

3 Basser PJ, Mattiello J, LeBihan D. Estimation of the effective self-diffusion tensor from the NMR spin echo. Journal of Magnetic Resonance. Series B. San Diego Cal 103.1994, 247–254.

4 Sulston JE, et al. The Embryonic Cell Lineage of the Nematode Caenorhabditis elegans. Developmental Biology 100, 64-119 (1983).

5 Towlson EK et al. The rich club of the C. elegans neuronal connectome. J Neurosci. 2013 Apr 10;33(15):6380-7.

6 Majka P et al. Towards a comprehensive atlas of cortical connections in a primate brain: Mapping tracer injection studies of the common marmoset into a reference digital template. J Comp Neurol. 2016 Aug 1;524(11):2161-81.

7 Zingg B, Hintiryan H, Gou L, Song MY, Bay M, Bienkowski MS, Foster NN, Yamashita S, Bowman I, Toga AW, Dong HW. Neural networks of the mouse neocortex. Cell 2014 156:1096–1111.

8 Biswal B, Yetkin FZ, Haughton VM, Hyde JS. Functional connectivity in the motor cortex of resting human brain using echo-planar MRI. Magn Reson Med. 1995 Oct; 34(4):537-41.

9 Wedeen VJ, Hagmann P, Tseng WY, Reese TG, Weisskoff RM. Mapping complex tissue architecture with diffusion spectrum magnetic resonance imaging. Magn. Reson. Med. 54, 1377–1386 (2005). (DSI).

10 Tuch D, Wedeen VJ, et al. High angular resolution diffusion imaging reveals intravoxel white matter fiber heterogeneity. MRM, 2002, 48(4):577-82.

11 Making connections. 396, Nature, vol 483, 22 March 2012.

12 Mansfield P. Multi-planar image formation using NMR spin echos. J. Phys. C, Solid State Physics 10:155 (1977).

13 Cohen MS, Weisskoff RM. Ultra-fast imaging. Magnetic Resonance Imaging 9:1 (1991).

14 Schmitt F et al. Echo-planar imaging of human brain perfusion at 1T. MRM: 116 (1991).

15 Turner R. A target field approach to optimal coil design. J Phys D 19:L147 (1986).

16 Siebold H. Gradient field coils for MR imaging with high spectral purity. IEEE Trans Magn 26:897 (1990).

17 Kimmlingen R, et al. Gradient System with Continously Variable Field Characteristics. Proc. Intl. Soc. Mag. Reson. Med. (1999).

18 Patz S et al. Novel encoding technology for ultrafast MRI in a limited spatial region. International Journal of Imaging Systems and Technology: 10.3:216 (1999).

19 Kaindl A, et al. Influence of chemo-rheological properties of silica-filled liquid epoxy resins on partial discharge behavior of coils. Proc. Coil Winding Conference (2001).

20 Irnich W. Electrostimulation by time-varying magnetic fields. MAGMA 2:43 (1994)

21 Kimmlingen R, et al. An easy to exchange high performance head gradient insert for a 3T whole body MRI system: First results. Proc. Intl. Soc. Mag. Reson. Med. (2004).

22 Takahashi E, Dai G, Wang R, Ohki K, Rosen GD, Galaburda AM, Grant PE, Wedeen VJ. Development of cerebral fiber pathways in cats revealed by diffusion spectrum imaging. Neuroimage 49(2): 1231-1240 (2010).

23 Kimmlingen R, et al. Concept and realization of high strength gradients for the Human Connectome Project. ISMRM conference (2012).

24 Budinger TF. Thresholds for physiological effects due to RF and magnetic fields used in NMR imaging. IEEE TransNucl.Sc., Vol. NS-26, No.2 April.1979.

25 Larkman DJ, Hajnal JV, Herlihy AH, Coutts GA, Young IR, Ehnholm G. Use of multicoil arrays for separation of signal from multiple slices simultaneously excited. J Magn Reson Imaging. 2001;13(2):313–317.

26 Feinberg DA, et al. Multiplexed Echo Planar Imaging for Sub-Second Whole Brain FMRI and Fast Diffusion Imaging. PLoS ONE, 2010. 5(12): p. e15710.

27 Setsompop K, Gagoski BA, Polimeni JR, Witzel T, Wedeen VJ, Wald LL. Blipped-controlled aliasing in parallel imaging for simultaneous multislice echo planar imaging with reduced g-factor penalty. Magn Reson Med. 2012 May; 67(5):1210-24.

28 Keil B, Blau JN, Biber S, Hoecht P, Tountcheva V, Setsompop K, Triantafyllou C, Wald LL. A 64-channel 3T array coil for accelerated brain MRI. Magn Reson Med. 2013 Jul; 70(1):248-58.

29 Setsompop K, Kimmlingen R, Eberlein E, Witzel T, Cohen-Adad J, McNab JA, Keil B, Tisdall MD, Hoecht P, Dietz P, Cauley SF, Tountcheva V, Matschl V, Lenz VH, Heberlein K, Potthast A, Thein H, Van Horn J, Toga A, Schmitt F, Lehne D, Rosen BR, Wedeen V, Wald LL. Pushing the limits of in vivo diffusion MRI for the Human Connectome Project. Neuroimage. 2013 Oct 15;80:220-33.

30 Fan Q, Nummenmaa A, Witzel T, Zanzonico R, Keil B, Cauley S, Polimeni JR, Tisdall D, Van Dijk K, Buckner RL, Wedeen V, Rosen BR, Wald LL. Investigating the capability to resolve complex white matter structures with high b-value diffusion MRI on the MGH-USC Connectome Scanner. Brain Connectivity, 2014 Nov; 4(9) p.718-26 PMID 25287963.

31 Van Wedeen J, Rosene DL, Wang R, Dai G, Mortazavi F, Hagmann P, Kaas JH, Tseng W-Y I. The Geometric Structure of the Brain Fiber Pathways: A Continuous Orthogonal Grid. Science. 2012 Mar 30; 335(6076): 1628–1634.
32 Huang SY, Nummenmaa A, Witzel T, Duval T, Cohen-Adad J, Wald LL, McNab JA. The impact of gradient strength on in vivo diffusion MRI estimates of axon diameter. Neuroimage 2014 Dec.9 Epub ahead of print. PMID: 25498429.
33 Huang, SY, Tobyne SM, Nummenmaa A, Witzel T, Wald LL, McNab JA, Klawiter EC Characterization of Axonal Disease in Patients with Multiple Sclerosis Using High-Gradient-Diffusion MR Imaging.
34 McNab JA, Edlow BL, Witzel T, Huang SY, Bhat H, Heberlein K, Feiweier T, Liu K, Keil B, Cohen-Adad J, Tisdall MD, Folkerth RD, Kinney HC, Wald LL. The Human Connectome Project and beyond: initial applications of 300 mT/m gradients. Neuroimage 2013;80:234-245.
35 Fan Q, Witzel T, Nummenmaa A, Van Dijk KR, Van Horn JD, Drews MK, Somerville LH, Sheridan MA, Santillana RM, Snyder J, Hedden T, Shaw EE, Hollinshead MO, Renvall V, Zanzonico R, Keil B, Cauley S, Polimeni JR, Tisdall D, Buckner RL, Wedeen VJ, Wald LL, Toga AW, Rosen BR. MGH-USC Human Connectome Project datasets with ultra-high b-value diffusion MRI. Neuroimage 2016;124(Pt B):1108-1114.

Contact

Ralph Kimmlingen, Ph.D.
Siemens Healthcare GmbH
Am Röthelheimpark 2
91052 Erlangen
Germany
ralph.kimmlingen@siemens-healthineers.com

36 Smith SM, Miller KL, Moeller S, Xu J, Auerbach EJ, Woolrich MW, Beckmanna CF, Jenkinson M, Andersson J, Glasser MF, Van Essen DC, Feinberg DA, Yacoub ES, Ugurbil K. Temporally-independent functional modes of spontaneous brain activity. www.pnas.org/cgi/doi/10.1073/pnas.1121329109, 2011.
37 Van Essen DC, et al. The Human Connectome Project: A data acquisition perspective. NeuroImage (2012), j.neuroimage.2012.02.018.
38 Ugurbil K, et al. Pushing spatial and temporal resolution for functional and diffusion MRI in the Human Connectome Project. Neuroimage 80, 80–104 (2013).
39 Van Essen DC, et al. The WU-Minn Human Connectome Project: an overview. Neuroimage 80, 62–79 (2013).
40 Sotiropoulos SN, Jbabdi S, Xu J, Andersson JL, Moeller S, Auerbach EJ, Glasser MF, Hernandez M, Sapiro G, Jenkinson M, Feinberg DA, Yacoub E, Lenglet C, Van Essen DC, Ugurbil K, Behrens TE. Advances in diffusion MRI acquisition and processing in the Human Connectome Project. Neuroimage. 2013 Oct 15; 80:125-43.
41 Glasser MF, Coalson TS, Robinson EC, Hacker CD, Harwell J, Yacoub E, Ugurbil K, Andersson J, Beckmann CF, Jenkinson M, Smith SM, Van Essen DC. A multi-modal parcellation of human cerebral cortex. Nature 536, 171–178 (11 August 2016).
42 Vu AT, Auerbach E, Lenglet C, Moeller S, Sotiropoulos SN, Jbabdi S, Andersson J, Yacoub E, Ugurbil K. High resolution whole brain diffusion imaging at 7 T for the Human Connectome Project. Neuroimage. 2015 Nov 15; 122: 318–331.
43 Vu AT. High resolution whole brain diffusion imaging at 7T for the Human Connectome Project. NeuroImage (2016), http://dx.doi.org/10.1016/j.neuroimage.2016.11.049.
44 Glasser MF, Smith SM, Marcus DS, Andersson JLR, Auerbach EJ, Behrens TEJ, Coalson TS, Harms MP, Jenkinson M, Moeller S, Robinson EC, Sotiropoulos SN, Xu J, Yacoub E, Ugurbil K, Van Essen DC. The Human Connectome Project's neuroimaging approach. Nature Neuroscience 19, 1175–1187 (2016).

MAGNETOM World

The Siemens Healthineers MR User Community

MAGNETOM Flash articles

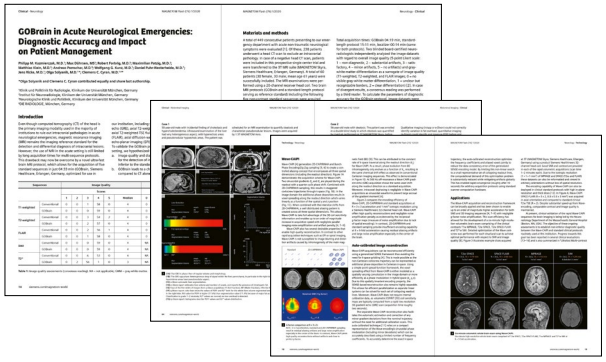

Lectures on all aspects of MRI

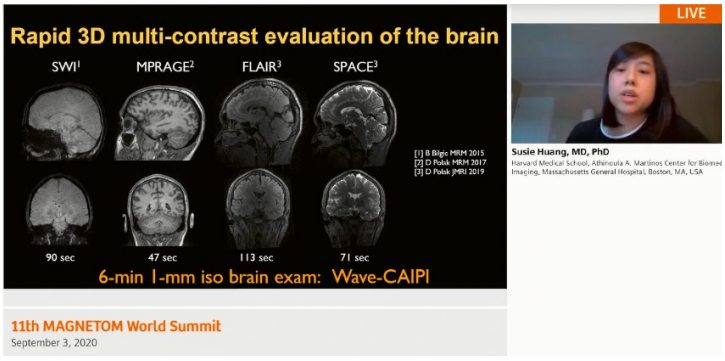

Application Tips and Protocols

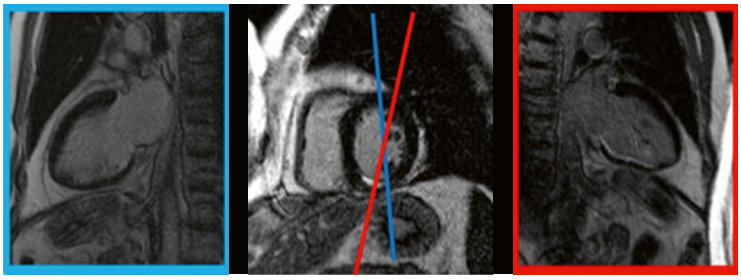

.edx .exar1

www.siemens-healthineers.com/magnetom-world

SIEMENS Healthineers

On account of certain regional limitations of sales rights and service availability, we cannot guarantee that all products included in this brochure are available through the Siemens sales organization worldwide. Availability and packaging may vary by country and is subject to change without prior notice. Some/All of the features and products described herein may not be available in the United States.

The information in this document contains general technical descriptions of specifications and options as well as standard and optional features which do not always have to be present in individual cases, and which may not be commercially available in all countries.

Due to regulatory reasons their future availability cannot be guaranteed. Please contact your local Siemens organization for further details.

Siemens reserves the right to modify the design, packaging, specifications, and options described herein without prior notice. Please contact your local Siemens sales representative for the most current information.

Note: Any technical data contained in this document may vary within defined tolerances. Original images always lose a certain amount of detail when reproduced.

Siemens Healthineers Headquarters
Siemens Healthcare GmbH
Henkestr. 127
91052 Erlangen, Germany
Phone: +49 9131 84-0
siemens-healthineers.com

Published by Siemens Healthcare GmbH · Order No. A91MR-1000-151C-7600 · Printed in Germany · 12103 0422 · ©Siemens Healthcare GmbH, 2022

siemens-healthineers.com/magnetom-world